

# Low Rank Independence Samplers in Bayesian Inverse Problems

D. Andrew Brown<sup>\*</sup>      Arvind Saibaba<sup>†</sup>      Sarah Vallélian<sup>‡</sup>

September 2, 2022

## Abstract

In Bayesian inverse problems, the posterior distribution is used to quantify uncertainty about the reconstructed solution. In practice, Markov chain Monte Carlo algorithms often are used to draw samples from the posterior distribution. However, implementations of such algorithms can be computationally expensive. We present a computationally efficient scheme for sampling high-dimensional Gaussian distributions in ill-posed Bayesian linear inverse problems. Our approach uses Metropolis-Hastings independence sampling with a proposal distribution based on a low-rank approximation of the prior-preconditioned Hessian. We show the dependence of the acceptance rate on the number of eigenvalues retained and discuss conditions under which the acceptance rate is high. We demonstrate our proposed sampler by using it with Metropolis-Hastings-within-Gibbs sampling in numerical experiments in image deblurring and computerized tomography.

**Keywords:** Computerized tomography, image deblurring, low rank approximation, Metropolis-Hastings independence sampler, prior-preconditioned Hessian

## 1 Introduction

Inverse problems aim to recover quantities that cannot be directly observed, but can only be measured indirectly and in the presence of measurement error. Such problems arise in many applications in science and engineering, including medical imaging [32], earth sciences [3], and particle physics [45]. The deterministic approach to inverse problems involves minimizing an objective function to obtain a point estimate of the unknown parameter. Inverse problems also admit a Bayesian interpretation, facilitating the use of prior information and allowing full quantification of uncertainty about the solutions in the form of a posterior probability distribution. An overview of Bayesian approaches to inverse problems is available in [37, 43, 64]. A recent special issue of *Inverse Problems* also highlights the advances in the Bayesian approach and the broad impacts of its applicability [14].

In the Bayesian statistical framework, the parameters of interest,  $\mathbf{x}$ , and the observed data,  $\mathbf{b}$ , are modeled as random variables. *A priori* uncertainty about the parameters is quantified in the prior distribution,  $\pi(\mathbf{x})$ . Bayesian inference then proceeds by updating the information about these parameters given the observed data. The updated information is quantified in the posterior distribution obtained via Bayes' rule  $\pi(\mathbf{x}|\mathbf{b}) \propto f(\mathbf{b}|\mathbf{x})\pi(\mathbf{x})$ , where  $f(\cdot|\mathbf{x})$  is the assumed data generating model determined by the forward operator and  $\mathbf{x}$ , also called the likelihood function. Rather than providing a single solution to the inverse problem, the Bayesian approach provides a distribution of plausible solutions, thereby enabling uncertainty quantification. Sampling from the posterior distribution

<sup>\*</sup>Department of Mathematical Sciences, Clemson University, Clemson, SC 29634; ab7@clemson.edu;

<sup>†</sup>Department of Mathematics, North Carolina State University, Raleigh, NC 27695; asaibab@ncsu.edu;

<sup>‡</sup>Statistical and Applied Mathematical Sciences Institute, Research Triangle Park, NC 27709; svallelian@samsi.info;

allows for simultaneous estimation of quantities of interest, as well as quantifying the associated uncertainty.

A challenge of the fully Bayesian approach is that the posterior distribution will usually not have a closed form, in which case sampling based approximations are often used to explore this distribution. The most common set of techniques for sampling from the posterior distribution is Markov chain Monte Carlo (MCMC) [22, 53]. Several MCMC methods for sampling the posterior distributions obtained from inverse problems have been proposed in the literature [6, 19, 8, 1, 9]. However, these methods can be computationally expensive on large-scale problems due to the need to factorize a large covariance matrix at each iteration; though there are cases in which the choice of the prior and the forward operator lead to a reduction in computational cost [7].

Our aim in this work is to address the computational burden posed by repeatedly sampling high dimensional Gaussian random variables as part of a larger MCMC routine. We do so by leveraging the low-rank structure of forward models typically encountered in linear inverse problems. Specifically, we propose a Metropolis-Hastings independence sampler, called LRIS<sup>1</sup>, in which the proposal distribution, based on a low-rank approximation to the prior-preconditioned Hessian, is easy to construct and to sample. We also develop a proposal distribution using a randomized approach for computing the low-rank approximation when doing so directly is computationally expensive. We derive explicit formulas for the acceptance rates of our proposed approaches and analyze their statistical properties. We provide a detailed description of the computational costs. Numerical experiments on image deblurring and computerized tomography support the theoretical properties of our proposed approaches and demonstrate the computational benefits over standard block Gibbs sampling [27].

The rest of the paper is organized as follows. In Section 2, we formulate a general linear inverse problem in the hierarchical Bayesian framework with particular attention paid to the computational bottleneck arising in standard MCMC samplers. In Section 3, we present our proposed approach of using low rank approximations as the basis of an independence sampler to accelerate drawing realizations from high-dimensional Gaussian distributions. In Section 4, we demonstrate the performance of our approach on simulated examples in image deblurring and CT reconstruction via Metropolis-Hastings-within-Gibbs sampling. The paper concludes with a discussion in Section 5 and proofs of stated results in an Appendix.

## 2 The Bayesian Statistical Inverse Problem

Assume that the observed data are corrupted by additive noise so that the stochastic model for the forward problem is

$$\mathbf{b} = \mathbf{A}\mathbf{x} + \boldsymbol{\epsilon}, \quad (1)$$

where  $\mathbf{A} \in \mathbb{R}^{m \times n}$  is the forward operator, or the parameter-to-observation map,  $\boldsymbol{\epsilon}$  is the measurement error, and  $\mathbf{x}$  is the underlying quantity that we wish to reconstruct. We suppose that observational noise  $\boldsymbol{\epsilon}$  is a Gaussian random variable with mean zero and covariance  $\mu^{-1}\mathbf{I}$ , independent of the unknown  $\mathbf{x}$ . In some applications,  $\mu$  may be known. Quite often, however, it is unknown and we assume that is the case here. Under this model,  $\mathbf{b} \mid \mathbf{x}, \mu \sim \mathcal{N}(\mathbf{A}\mathbf{x}, \mu^{-1}\mathbf{I})$  so that the likelihood is

$$f(\mathbf{b} \mid \mathbf{x}, \mu) \propto \mu^{m/2} \exp\left(-\frac{\mu}{2}(\mathbf{b} - \mathbf{A}\mathbf{x})^\top(\mathbf{b} - \mathbf{A}\mathbf{x})\right), \quad \mathbf{b} \in \mathbb{R}^m. \quad (2)$$

The prior distribution for  $\mathbf{x}$  encodes the structure we expect or wish to enforce on  $\mathbf{x}$  before taking observed data into account. An often reasonable prior for  $\mathbf{x}$  is Gaussian with mean zero and covariance  $\sigma^{-1}\boldsymbol{\Gamma}_{\text{pr}} \equiv \sigma^{-1}(\mathbf{L}^\top \mathbf{L})^{-1}$ ; i.e.,

$$\pi(\mathbf{x} \mid \sigma) \propto \sigma^{n/2} \exp\left(-\frac{\sigma}{2}\mathbf{x}^\top \boldsymbol{\Gamma}_{\text{pr}}^{-1} \mathbf{x}\right), \quad \mathbf{x} \in \mathbb{R}^n, \quad (3)$$

where the covariance matrix  $\boldsymbol{\Gamma}_{\text{pr}}$  is assumed known up to the precision  $\sigma$ .

---

<sup>1</sup>Pronounced “ell”ris

Different covariance matrices may be chosen depending on what structure one wishes to enforce on the estimand  $\mathbf{x}$ . A popular choice is a Gaussian process (GP) [51]. Several choices of covariance kernel for the GP are available, with the most common being in the Matérn family. The prior structure we use in our numerical experiments (Section 4) is motivated by Gaussian Markov random fields (GMRFs) [55]. In this approach, the precision matrix is expressed as the discretized representation of the differential operator  $(\kappa^2 - \Delta)^{\alpha/2}$ , where  $\alpha = \nu + d/2$ ,  $\nu$  is the smoothness parameter of the Matérn kernel, and  $d$  is the dimension. An explicit connection between GPs and GMRFs is presented in [40]. An advantage of the GMRF representation is that the precision matrix is sparse and thus computationally efficient to handle when  $\alpha$  is an even integer. GPs, on the other hand, more easily accommodate stationarity and generally allow for smoother fields. However, GP covariance kernels have infinite support so that the resulting covariance matrices are dense, creating challenges for large-scale applications. Fast Fourier Transform-based approaches on regular grids (e.g., [2]) and the  $\mathcal{H}$ -matrix approach on irregular grids (e.g., [57, 58]), though, can make the computational costs comparable to those associated with GMRFs.

Conditional on  $\mu$  and  $\sigma$ , we have  $\mathbf{x} \mid \mathbf{b}, \mu, \sigma \sim \mathcal{N}(\mathbf{x}_{\text{cond}}, \mathbf{\Gamma}_{\text{cond}})$ , where  $\mathbf{\Gamma}_{\text{cond}} = (\mu \mathbf{A}^\top \mathbf{A} + \sigma \mathbf{\Gamma}_{\text{pr}}^{-1})^{-1}$  and  $\mathbf{x}_{\text{cond}} = \mu \mathbf{\Gamma}_{\text{cond}} \mathbf{A}^\top \mathbf{b}$ ; i.e.,

$$\pi(\mathbf{x} \mid \mathbf{b}, \mu, \sigma) \propto \exp \left( -\frac{\mu}{2} \|\mathbf{A}\mathbf{x} - \mathbf{b}\|_2^2 - \frac{\sigma}{2} \|\mathbf{L}\mathbf{x}\|_2^2 \right). \quad (4)$$

The conditional posterior mode,  $\hat{\mathbf{x}} = \arg \max_{\mathbf{x} \in \mathbb{R}^n} \pi(\mathbf{x} \mid \mathbf{b}, \mu, \sigma)$ , is the minimizer of the negative log-likelihood  $(\mu/2) \|\mathbf{A}\mathbf{x} - \mathbf{b}\|_2^2 + (\sigma/2) \|\mathbf{L}\mathbf{x}\|_2^2$  and thus corresponds to Tikhonov regularization in the deterministic linear inverse problem.

In the formulation of the inverse problem specified by equations (2) and (3) and with a prior  $\pi(\mu, \sigma)$  on  $\mu$  and  $\sigma$ , the joint posterior density is given by

$$\pi(\mathbf{x}, \mu, \sigma \mid \mathbf{b}) \propto \mu^{m/2} \sigma^{n/2} \exp \left( -\frac{\mu}{2} \|\mathbf{A}\mathbf{x} - \mathbf{b}\|_2^2 - \frac{\sigma}{2} \|\mathbf{L}\mathbf{x}\|_2^2 \right) \pi(\mu, \sigma). \quad (5)$$

In our numerical experiments in Section 4 we consider two different priors on the precision parameters, conditionally conjugate Gamma distributions and a weakly informative prior.

With the priors on the precision components, the full posterior distribution is no longer Gaussian and generally not available in closed form. Many different techniques are available for approximating complicated probability distributions. Since the seminal work of Gelfand and Smith [22], Markov chain Monte Carlo, particularly Gibbs sampling, has become the predominant technique for Bayesian computation. A version of the basic block Gibbs sampling algorithm for sampling from (5) is given in Algorithm 1. Most often,  $\mu$  and  $\sigma$  are updated individually (especially when using conditionally conjugate Gamma priors), but this is not necessary. Typically,  $\mathbf{x}$  is drawn separate from  $(\mu, \sigma)$  to take advantage of its conditionally conjugate Gaussian distribution. An early modification of Gibbs sampling is the so-called Metropolis-Hastings-within-Gibbs to deal with challenging full conditional distributions [44].

Typically, for any iterative sampling algorithm in the Bayesian linear inverse problem, the computational cost per iteration is dominated by the cost of sampling  $\mathbf{x} \mid \mathbf{b}, \mu, \sigma$  in (4). While sampling from this Gaussian distribution is a very straightforward procedure, the fact that it is high-dimensional makes it very computationally intensive. To circumvent the computational burden, we propose substituting direct sampling with a Metropolis-Hastings independence sampler using a computationally cheap low-rank proposal distribution. We present our proposed approach in Section 3.

### 3 Independence Sampling with Low-Rank Proposals

Here we briefly review independence sampling and discuss a proposal distribution that uses a low-rank approximation to efficiently generate samples from (4).

**Input:** Full conditional distributions of  $\mathbf{x} \mid \mathbf{b}, \mu, \sigma$  and  $(\mu, \sigma) \mid \mathbf{x}, \mathbf{b}$ , sample size  $N$ , burn-in period  $N_b$ .

**Output:** Approximate sample from the posterior distribution (5),  $\{\mathbf{x}_{(t)}, \mu_{(t)}, \sigma_{(t)}\}_{t=N_b+1}^N$ .

```

1 Initialize  $\mathbf{x}_{(0)}, \mu_{(0)}$ , and  $\sigma_{(0)}$ .
2 for  $t = 1$  to  $N$  do
3   Draw  $\mathbf{x}_{(t)} \sim \mathcal{N}(\mu_{(t-1)}\mathbf{\Gamma}_{\text{cond}}^{(t)}\mathbf{A}^\top\mathbf{b}, \mathbf{\Gamma}_{\text{cond}}^{(t)})$ , where  $\mathbf{\Gamma}_{\text{cond}}^{(t)} = (\mu_{(t-1)}\mathbf{A}^\top\mathbf{A} + \sigma_{(t-1)}\mathbf{\Gamma}_{\text{pr}}^{-1})^{-1}$ .
4   Draw  $(\mu_{(t)}, \sigma_{(t)}) \sim \mu, \sigma \mid \mathbf{x}_{(t)}, \mathbf{b}$ .
5 end

```

**Algorithm 1:** An outline of the standard block Gibbs algorithm for sampling the posterior density (5).

### 3.1 Independence Sampling

Let  $\boldsymbol{\theta} \in \mathbb{R}^n$  and denote the (possibly unnormalized) target density by  $h(\boldsymbol{\theta})$ . The Metropolis-Hastings (MH) algorithm [42, 31] proceeds iteratively by generating at iteration  $t$  a draw,  $\boldsymbol{\theta}_*$ , from an available proposal distribution possibly conditioned on the current state,  $\boldsymbol{\theta}_{(t-1)}$ , and setting  $\boldsymbol{\theta}_{(t)} = \boldsymbol{\theta}_*$  with probability

$$\alpha(\boldsymbol{\theta}_{(t-1)}, \boldsymbol{\theta}_*) = \min \left\{ \frac{h(\boldsymbol{\theta}_*)q(\boldsymbol{\theta}_{(t-1)} \mid \boldsymbol{\theta}_*)}{h(\boldsymbol{\theta}_{(t-1)})q(\boldsymbol{\theta}_* \mid \boldsymbol{\theta}_{(t-1)})}, 1 \right\}, \quad (6)$$

where  $q(\cdot \mid \boldsymbol{\theta}_{(t-1)})$  is the density of the proposal distribution. This algorithm produces a Markov chain  $\{\boldsymbol{\theta}_{(t)}\}$  with transition kernel

$$K(\boldsymbol{\theta}, \boldsymbol{\theta}_*) = \alpha(\boldsymbol{\theta}, \boldsymbol{\theta}_*)q(\boldsymbol{\theta}_* \mid \boldsymbol{\theta}) + \delta_{\boldsymbol{\theta}}(\boldsymbol{\theta}_*) \left( 1 - \int \alpha(\boldsymbol{\theta}, \boldsymbol{\theta}')q(\boldsymbol{\theta}' \mid \boldsymbol{\theta})d\boldsymbol{\theta}' \right),$$

where  $\delta_{\boldsymbol{\theta}}(\cdot)$  is the point mass at  $\boldsymbol{\theta}$ . Properties of the MH algorithm, including convergence to the target distribution, may be found in [53] and elsewhere.

An independence Metropolis-Hastings sampler (IMHS) proposes states from a density that is independent of the current state of the chain. The proposal has density  $q(\boldsymbol{\theta}_* \mid \boldsymbol{\theta}_{(t-1)}) \equiv g(\boldsymbol{\theta}_*)$ , and the ratio in (6) can be written as

$$\frac{h(\boldsymbol{\theta}_*)g(\boldsymbol{\theta}_{(t-1)})}{h(\boldsymbol{\theta}_{(t-1)})g(\boldsymbol{\theta}_*)} = \frac{w(\boldsymbol{\theta}_*)}{w(\boldsymbol{\theta}_{(t-1)})}, \quad (7)$$

where  $w(\boldsymbol{\theta}) \propto h(\boldsymbol{\theta})/g(\boldsymbol{\theta})$ . The IMHS is similar to the *rejection algorithm*. The rejection algorithm draws a candidate value  $\boldsymbol{\theta}_*$  from an available generating distribution with density  $g$  such that for some  $M \geq 1$ ,  $h(\boldsymbol{\theta}) \leq Mg(\boldsymbol{\theta})$ , for all  $\boldsymbol{\theta}$ , then accepts the draw with probability  $h(\boldsymbol{\theta}_*)/Mg(\boldsymbol{\theta}_*)$ , resulting in an exact draw from the target distribution.

For both the IMHS and rejection sampler, it is desirable for  $g$  to match the target density as closely as possible and, hence, to have an acceptance rate as high as possible. At least,  $g$  should generally follow  $h$ , but with tails that are no lighter than  $h$  [25, 53]. These guidelines are in contrast to those prescribed for the more common random walk MH, in which the best convergence is generally obtained with acceptance rates between 20% and 50% [25, 54]. In the sequel, we discuss our proposed generating distribution both as an independence sampler as well as its use in a rejection algorithm.

### 3.2 Approximating the Target Distribution

Samples from the conditional distribution  $\mathcal{N}(\mathbf{x}_{\text{cond}}, \mathbf{\Gamma}_{\text{cond}})$  can be generated as  $\mathbf{x} = \mathbf{x}_{\text{cond}} + \mathbf{G}\boldsymbol{\epsilon}$ , where  $\boldsymbol{\epsilon} \sim \mathcal{N}(\mathbf{0}, \mathbf{I})$  and  $\mathbf{G}$  satisfies  $\mathbf{\Gamma}_{\text{cond}} = \mathbf{G}\mathbf{G}^\top$ . Forming the mean  $\mathbf{x}_{\text{cond}}$  and computing the

random vector  $\mathbf{G}\epsilon$  involve expensive operations with the covariance matrix. By leveraging the low-rank nature of the forward operator  $\mathbf{A}$ , though, we can construct a fast proposal distribution for an independence sampler.

Consider the covariance matrix  $\mathbf{\Gamma}_{\text{cond}} = (\mu\mathbf{A}^\top\mathbf{A} + \sigma\mathbf{L}^\top\mathbf{L})^{-1}$ . Factorizing this matrix so that

$$\mathbf{\Gamma}_{\text{cond}} = \mathbf{L}^{-1}(\mu\mathbf{L}^{-\top}\mathbf{A}^\top\mathbf{A}\mathbf{L}^{-1} + \sigma\mathbf{I})^{-1}\mathbf{L}^{-\top} \quad (8)$$

yields the so-called *prior-preconditioned Hessian transformation*  $\mathbf{H} := \mathbf{L}^{-\top}\mathbf{A}^\top\mathbf{A}\mathbf{L}^{-1}$  [13, 18, 48, 58]. For highly ill-posed inverse problems such as those considered here,  $\mathbf{A}$  either has a rapidly decaying spectrum or is rank deficient. The product singular value inequalities [34, Theorem 3.3.16 (b)] ensure that  $\mathbf{A}\mathbf{L}^{-1}$  has the same rank as  $\mathbf{A}$  and the same rate of decay of singular values. A detailed discussion on the low-rank approximation of the prior-preconditioned Hessian is provided in [18, Section 3].

We approximate  $\mathbf{H}$  using a truncated eigenvalue decomposition,

$$\mathbf{L}^{-\top}\mathbf{A}^\top\mathbf{A}\mathbf{L}^{-1} \approx \mathbf{V}_k\mathbf{\Lambda}_k\mathbf{V}_k^\top, \quad (9)$$

where  $\mathbf{V}_k \in \mathbb{R}^{n \times k}$  has orthonormal columns and  $\mathbf{\Lambda}_k \in \mathbb{R}^{k \times k}$  is the diagonal matrix containing the  $k \leq n$  largest eigenvalues of  $\mathbf{H}$ . If  $\text{rank}(\mathbf{A}) = k$ , then exact equality holds. The truncation parameter  $k$  controls the tradeoff between accuracy on the one hand and computational and memory costs on the other hand.

We can approximate the conditional covariance matrix  $\mathbf{\Gamma}_{\text{cond}}$  by substituting (9) into (8),

$$\hat{\mathbf{\Gamma}}_{\text{cond}} \equiv \mathbf{L}^{-1} \frac{1}{\sigma} (\mathbf{I} + \frac{\mu}{\sigma} \mathbf{V}_k \mathbf{\Lambda}_k \mathbf{V}_k^\top)^{-1} \mathbf{L}^{-\top}. \quad (10)$$

Using the Woodbury identity and the fact that  $\mathbf{V}_k$  has orthonormal columns, the right-hand side of (10) becomes

$$\hat{\mathbf{\Gamma}}_{\text{cond}} = \frac{1}{\sigma} \mathbf{L}^{-1} (\mathbf{I} - \mathbf{V}_k \mathbf{D}_k \mathbf{V}_k^\top) \mathbf{L}^{-\top}, \quad \mathbf{D}_k = \text{diag}(\mu\lambda_j(\mu\lambda_j + \sigma)^{-1} : j = 1, \dots, k) \in \mathbb{R}^{k \times k},$$

where  $\lambda_j$ ,  $j = 1, \dots, k$ , are the diagonals of  $\mathbf{\Lambda}_k$ . To approximate the mean  $\mathbf{x}_{\text{cond}}$ , replace  $\mathbf{\Gamma}_{\text{cond}}$  by  $\hat{\mathbf{\Gamma}}_{\text{cond}}$  so that  $\hat{\mathbf{x}}_{\text{cond}} = \mu\hat{\mathbf{\Gamma}}_{\text{cond}}\mathbf{A}^\top\mathbf{b}$ . With these approximations, the proposal distribution for our proposed independence sampler is  $\mathcal{N}(\hat{\mathbf{x}}_{\text{cond}}, \hat{\mathbf{\Gamma}}_{\text{cond}})$ . The optimality of this low-rank approximation was studied in [63].

A factorization of the form  $\hat{\mathbf{\Gamma}}_{\text{cond}} = \mathbf{G}\mathbf{G}^\top$  can be used to sample from  $\mathcal{N}(\hat{\mathbf{x}}_{\text{cond}}, \hat{\mathbf{\Gamma}}_{\text{cond}})$ . It can be verified that

$$\mathbf{G} := \frac{1}{\sqrt{\sigma}} \mathbf{L}^{-1} (\mathbf{I} - \mathbf{V}_k \hat{\mathbf{D}}_k \mathbf{V}_k^\top), \quad \hat{\mathbf{D}}_k = \mathbf{I} \pm (\mathbf{I} - \mathbf{D}_k)^{1/2},$$

satisfies  $\hat{\mathbf{\Gamma}}_{\text{cond}} = \mathbf{G}\mathbf{G}^\top$ . Since  $\hat{\mathbf{D}}_k$  is diagonal and  $k \ll n$ , we obtain a computationally cheap way of generating draws from the high-dimensional proposal distribution  $\mathcal{N}(\hat{\mathbf{x}}_{\text{cond}}, \hat{\mathbf{\Gamma}}_{\text{cond}})$ . Then we can use a Metropolis-Hastings step to correct for the approximation. This results in our proposed LRIS algorithm.

### 3.3 Analysis of Acceptance Ratio

Here, we derive an explicit formula for evaluating the acceptance ratio for our proposed algorithm and provide insight into the conditions for which the proposal distribution  $\mathcal{N}(\hat{\mathbf{x}}_{\text{cond}}, \hat{\mathbf{\Gamma}}_{\text{cond}})$  closely approximates the target distribution  $\mathcal{N}(\mathbf{x}_{\text{cond}}, \mathbf{\Gamma}_{\text{cond}})$ . For simplicity of notation, we drop the conditioning on  $\mathbf{b}, \mu$  and  $\sigma$ . The target density is

$$h(\mathbf{x}) := \frac{1}{\sqrt{(2\pi)^n \det(\mathbf{\Gamma}_{\text{cond}})}} \exp\left(-\frac{1}{2}(\mathbf{x} - \mathbf{x}_{\text{cond}})^\top \mathbf{\Gamma}_{\text{cond}}^{-1}(\mathbf{x} - \mathbf{x}_{\text{cond}})\right), \quad (11)$$

and the proposal density,  $g(\mathbf{x})$ , replaces  $\mathbf{x}_{\text{cond}}$  by  $\hat{\mathbf{x}}_{\text{cond}}$  and  $\mathbf{\Gamma}_{\text{cond}}$  by  $\hat{\mathbf{\Gamma}}_{\text{cond}}$  in the density  $h(\mathbf{x})$ . The following result gives a practical way to compute the acceptance ratio. It can be verified with a little algebra, so the proof is omitted.

**Proposition 1.** *The LRIS acceptance ratio can be computed as  $\eta(\mathbf{z}, \mathbf{x}) = w(\mathbf{z})/w(\mathbf{x})$ , where*

$$w(\mathbf{x}) = \exp\left(-\frac{1}{2}\mathbf{x}^\top(\mathbf{\Gamma}_{\text{cond}}^{-1} - \hat{\mathbf{\Gamma}}_{\text{cond}}^{-1})\mathbf{x}\right).$$

An efficient implementation and the cost of computing this ratio is discussed in Subsection 3.5. The quality of the low-rank approximation to the target distribution can be seen through the acceptance ratio.

**Proposition 2.** *The LRIS acceptance ratio can be expressed as*

$$\eta(\mathbf{z}, \mathbf{x}) = \exp\left(-\frac{\mu}{2} \sum_{j=k+1}^n \lambda_j \left[(\mathbf{v}_j^\top \mathbf{L}\mathbf{z})^2 - (\mathbf{v}_j^\top \mathbf{L}\mathbf{x})^2\right]\right). \quad (12)$$

*Proof.* See Appendix A. □

This proposition asserts that the acceptance ratio is high when either  $\mu$  is small or the discarded eigenvalues  $\{\lambda_j\}_{j=k+1}^n$  are small. The dependence of the acceptance ratio on the eigenvectors can be seen explicitly by writing  $(\mathbf{v}_j^\top \mathbf{L}\mathbf{z})^2 - (\mathbf{v}_j^\top \mathbf{L}\mathbf{x})^2 = [\mathbf{v}_j^\top \mathbf{L}(\mathbf{z} + \mathbf{x})][\mathbf{v}_j^\top \mathbf{L}(\mathbf{z} - \mathbf{x})]$ . Thus, if  $\mathbf{z} \pm \mathbf{x} \perp \mathbf{L}^\top \mathbf{v}_j$ , then the acceptance ratio is 1.

While Proposition 2 provides insight into realizations of the acceptance ratio, the actual acceptance ratio is a random variable. The expected behavior and variability of this quantity can be understood through Theorem 1. To this end, define the constants

$$N_\ell := \exp\left(\frac{\mu^2}{2\sigma} \sum_{j=k+1}^n \frac{\ell\mu\lambda_j}{\ell\mu\lambda_j + \sigma} (\mathbf{b}^\top \mathbf{A}\mathbf{L}^{-1}\mathbf{v}_j)^2\right) \prod_{j=k+1}^n \left(1 + \frac{\ell\mu}{\sigma} \lambda_j\right)^{1/2}, \quad \ell = 1, 2, \dots \quad (13)$$

**Theorem 1.** *Let  $\mathbf{x}$  be the current state of the chain and let  $\mathbf{z}$  be the proposed state. Then the expected value and the variance of the acceptance ratio are given by*

$$\begin{aligned} e_\eta &:= \mathbb{E}_{\mathbf{z}|\mathbf{x}}[\eta(\mathbf{z}, \mathbf{x})] = \frac{1}{N_1 w(\mathbf{x})} \\ v_\eta^2 &:= \mathbb{V}_{\mathbf{z}|\mathbf{x}}[\eta(\mathbf{z}, \mathbf{x})] = \frac{1}{w^2(\mathbf{x})} \left(\frac{1}{N_2} - \frac{1}{N_1^2}\right). \end{aligned} \quad (14)$$

where  $\mathbb{E}_{\mathbf{z}|\mathbf{x}}(\cdot)$  denotes expectation conditional on  $\mathbf{x}$ , and  $\mathbb{V}_{\mathbf{z}|\mathbf{x}}(\cdot)$  denotes the variance conditional on  $\mathbf{x}$ .

*Proof.* See Appendix A. □

Using this result, a straightforward application of Chebyshev's inequality [52] shows that for any  $\epsilon > 0$ ,

$$\Pr_{\mathbf{z}|\mathbf{x}}\left(\left|\eta(\mathbf{z}, \mathbf{x}) - \frac{1}{N_1 w(\mathbf{x})}\right| \geq \epsilon\right) \leq \frac{1}{\epsilon^2 w^2(\mathbf{x})} \left(\frac{1}{N_2} - \frac{1}{N_1^2}\right), \quad (15)$$

where  $\Pr_{\mathbf{z}|\mathbf{x}}(\cdot)$  denotes probability conditional on the current state  $\mathbf{x}$  and we assume that  $w(\mathbf{x}) > 0$ . Thus, we can construct conditional prediction intervals about the realized acceptance rate. For instance, at any given state  $\mathbf{x}$ ,  $\Pr_{\mathbf{z}|\mathbf{x}}(\eta(\mathbf{z}, \mathbf{x}) \in [e_\eta \pm 4.47v_\eta]) \geq 0.95$ . In Appendix A, we derive expressions for all moments of the acceptance ratio.

It is clear from Theorem 1 that if the eigenvalues  $\{\lambda_j\}_{j=k+1}^n$  are zero, then the acceptance probability is 1. Likewise, if the eigenvalues are nonzero but small in magnitude, then the acceptance rate is close to 1. Further, consider the SVD of  $\mathbf{A}\mathbf{L}^{-1} = \mathbf{U}\mathbf{\Sigma}\mathbf{V}^\top$ . Then  $\mathbf{b}^\top \mathbf{A}\mathbf{L}^{-1} \mathbf{v}_j$  in (13) is equal to  $\sigma_j \mathbf{b}^\top \mathbf{u}_j$ , where  $\mathbf{u}_j$  is the  $j$ th singular vector of  $\mathbf{A}\mathbf{L}^{-1}$ . Thus, the acceptance rate may be close to 1 even if the components of the measurement  $\mathbf{b}$  along the left singular vectors of  $\mathbf{A}\mathbf{L}^{-1}$  are small. This is closely related to filter factors that are used to analyze deterministic inverse problems [30].

**Convergence and the Rejection Algorithm** Our proposed candidate generating distribution  $g(\mathbf{x})$  bounds the target distribution up to a fixed constant as a function of the remaining eigenvalues in the low-rank approximation, as verified by the next Proposition.

**Proposition 3.** *The target density  $h(\mathbf{x})$  (11) and the proposal density  $g(\mathbf{x})$  can be bounded as  $h(\mathbf{x}) \leq N_1 g(\mathbf{x})$  for all  $\mathbf{x}$ , where  $N_1 \geq 1$  is given in (13).*

*Proof.* See Appendix A. □

Proposition 3 establishes that the subchain produced by our proposed sampler has stationary distribution  $\pi(\cdot \mid \mathbf{b}, \mu, \sigma)$  and is uniformly ergodic by [53, Theorem 7.8]; i.e.,

$$\|K^p(\mathbf{x}, \cdot) - \pi(\cdot \mid \mathbf{b}, \mu, \sigma)\|_{TV} \leq 2(1 - N_1^{-1})^p \quad \forall \mathbf{x} \in \text{supp } \pi,$$

where  $K^p(\mathbf{x}, \cdot)$  is the  $p$ -step transition kernel starting from  $\mathbf{x}$  and  $\|\cdot\|_{TV}$  denotes the total variation norm. Thus, if one runs several sub-iterations of the LRIS, the realizations will converge to a draw from the true full conditional distribution at a rate independent of the initial state. Convergence is faster as the remaining eigenvalues from the low-rank approximation become small, and is immediate when the remaining eigenvalues are zero.

Proposition 3 suggests also that the approximating distribution can be used in a rejection algorithm instead of LRIS. The proof of this Proposition shows that  $\det(\widehat{\mathbf{\Gamma}}_{\text{cond}}) \geq \det(\mathbf{\Gamma}_{\text{cond}})$ , but each determinant is the generalized variance of its distribution [36]. When there are non-zero eigenvalues left out of the low-rank approximation, the proposal density will have heavier tails than the target density, a desirable property for a candidate distribution in a rejection algorithm [24]. Otherwise, the approximation is exact. We remark, however, that for a given candidate density  $g$ , LRIS is more efficient than a rejection algorithm in terms of variances of the concomitant estimators [41]. Further, the rejection sampler requires knowledge of  $N_1$ , which depends on eigenvalues that may be unavailable. Therefore, in our simulation study in Section 4, we use LRIS instead of rejection sampling.

### 3.4 Generating Low-Rank Approximations

The major cost of our proposed sampler is the precomputation cost in constructing the low-rank approximation. The standard approach for computing this low-rank approximation is to use a Krylov subspace solver (e.g., Lanczos method [56]) for computing a partial eigenvalue decomposition. Alternatively, we can compute the rank- $k$  singular value decomposition  $\mathbf{A}\mathbf{L}^{-1} \approx \mathbf{U}_k \mathbf{\Sigma}_k \mathbf{V}_k^\top$ . Then the approximate low-rank decomposition can be computed as  $\mathbf{H} \approx \mathbf{V}_k \mathbf{\Sigma}_k^2 \mathbf{V}_k^\top$ . Here we discuss a computationally efficient alternative for these computations.

Randomized SVD, reviewed in [28], is a computationally efficient approach for computing a low-rank approximation to the prior-preconditioned Hessian  $\mathbf{H}$ . The basic idea of the randomized SVD approach is to draw a random matrix  $\mathbf{\Omega} \in \mathbb{R}^{n \times (k+p)}$ , where the entries of  $\mathbf{\Omega}$  are i.i.d. standard Gaussian random variables. Here,  $k$  is the target rank and  $p$  is a small oversampling parameter. An approximation to the column space of  $\mathbf{H}$  is computed by the matrix product  $\mathbf{Y} = \mathbf{H}\mathbf{\Omega}$ . A thin-QR factorization  $\mathbf{Y} = \mathbf{Q}\mathbf{R}$  is computed, and the resulting low-rank approximation to  $\mathbf{H}$  is given by

$$\mathbf{H} \approx \widehat{\mathbf{H}} := \mathbf{Q}\mathbf{Q}^\top \mathbf{H}\mathbf{Q}\mathbf{Q}^\top. \quad (16)$$

**Input:** Matrix  $\mathbf{H} \in \mathbb{R}^{n \times n}$  and random matrix  $\mathbf{\Omega} \in \mathbb{R}^{n \times (k+p)}$ .  
**Output:** Approximate eigenvectors  $\mathbf{V}$  and approximate eigenvalues  $\mathbf{\Lambda}$ .  
**1** Compute  $\mathbf{Y} = \mathbf{H}\mathbf{\Omega}$  and thin-QR factorization  $\mathbf{Y} = \mathbf{Q}\mathbf{R}$ .  
**2** Compute  $\mathbf{T} = \mathbf{Q}^\top \mathbf{H}\mathbf{Q}$  and its eigendecomposition  $\mathbf{T} = \mathbf{U}\mathbf{\Lambda}\mathbf{U}^\top$ .  
**3** Compute  $\mathbf{V} = \mathbf{Q}\mathbf{U}$ .

**Algorithm 2:** Randomized SVD algorithm for computing low-rank decomposition.

This low-rank approximation can be postprocessed to obtain an approximate low-rank decomposition of the form (9). This is summarized in Algorithm 2.

Similar to Theorem 1, we can bound the expected value of the acceptance ratio using the randomized SVD approach.

**Theorem 2.** *Suppose we compute the low-rank approximation  $\widehat{\mathbf{H}}$  using Algorithm 2 with guess  $\mathbf{\Omega} \in \mathbb{R}^{n \times (k+p)}$ . Let  $p \geq 2$  be the oversampling parameter. Then*

$$\mathbb{E}_{\mathbf{\Omega}|\mathbf{z},\mathbf{x}} [\eta(\mathbf{z}, \mathbf{x})] \geq \exp \left( -\mu \|\mathbf{L}\mathbf{z}\|^2 \left[ \alpha \lambda_{k+1} + \beta \left( \sum_{j=k+1}^n \lambda_j^2 \right)^{1/2} \right] \right),$$

where  $\alpha = 1 + \sqrt{\frac{k}{p-1}}$ ,  $\beta = \frac{e\sqrt{k+p}}{p}$  and  $\mathbb{E}_{\mathbf{\Omega}|\mathbf{z},\mathbf{x}}$  denotes expectation w.r.t.  $\mathbf{\Omega}$  conditional on the current state  $\mathbf{x}$  and the proposed step  $\mathbf{z}$ .

*Proof.* See Appendix A. □

The interpretation of the result is the same as Theorem 1. That is, if the eigenvalues of the prior-preconditioned Hessian  $\mathbf{H}$  are rapidly decaying or zero beyond the index  $k$ , then the expected acceptance rate is high.

In practice, an oversampling parameter of  $p \lesssim 20$  is recommended [28]. As proposed, Algorithm 2 requires  $2(k+p)$  matrix-vector products (matvecs) with  $\mathbf{H}$ . This second round of matvecs required in Step 2 can be avoided by using the approximation [59, Section 2.3]

$$\mathbf{T} \approx (\mathbf{\Omega}^\top \mathbf{Q})^{-1} (\mathbf{\Omega}^\top \mathbf{Y}) (\mathbf{Q}^\top \mathbf{\Omega})^{-1}.$$

This is an example of the so-called single pass algorithm. Other single pass algorithms are discussed in [66]. In practice, the target rank  $k$  may not be known, in which case a modified approach may be used to adaptively estimate the subspace [28, Algorithm 4.2].

### 3.5 Computational Costs

Denote the computational cost of a matvec with  $\mathbf{A}$  by  $T_{\mathbf{A}}$ , and the cost of matvec with  $\mathbf{L}$  and  $\mathbf{L}^{-1}$  as  $T_{\mathbf{L}}$  and  $T_{\mathbf{L}^{-1}}$ , respectively. For simplicity, we assume the cost of the transpose operations of the respective matrices is the same as that of the original matrix.

It is difficult to accurately estimate the cost of the Krylov subspace method *a priori*, but the cost is roughly 2 sets of matvecs with  $\mathbf{A}$  and  $\mathbf{L}^{-1}$  and an additional  $\mathcal{O}(nk^2)$  operations. The quantities  $\mathbf{A}^\top \mathbf{b}$  and  $\mathbf{L}^{-\top} \mathbf{A}^\top \mathbf{b}$  can also be precomputed at a cost of  $T_{\mathbf{A}}$  and  $T_{\mathbf{A}} + T_{\mathbf{L}^{-1}}$  flops, respectively. Generally speaking, this is the same asymptotic cost for randomized SVD. In practice, however, randomized SVD can be much cheaper since it only seeks an approximate factorization [28].

The cost of computing the mean  $\hat{\mathbf{x}}_{\text{cond}}$  involves the application of  $\mathbf{L}^{-1}$  and  $(\mathbf{I} - \mathbf{V}_k \mathbf{D}_k \mathbf{V}_k^\top)$ . This costs  $T_{\mathbf{L}^{-1}} + 4nk$  flops. Similarly, the cost of  $\mathbf{G}\epsilon$  is also  $T_{\mathbf{L}^{-1}} + 4nk$  flops. The important point here is that generating a sample from the proposal distribution does not require a matvec with



Operation	Formula	Cost
Precomputation	Equation (9)	$2k(T_{\mathbf{A}} + T_{\mathbf{L}^{-1}}) + \mathcal{O}(nk^2)$
Computing mean	$\hat{\mathbf{x}}_{\text{cond}} = \mu \hat{\mathbf{\Gamma}}_{\text{cond}} \mathbf{A}^\top \mathbf{b}$	$T_{\mathbf{L}^{-1}} + 4nk$
Generating sample	$\mathbf{x} \sim \mathcal{N}(\hat{\mathbf{x}}_{\text{cond}}, \hat{\mathbf{\Gamma}}_{\text{cond}})$	$T_{\mathbf{L}^{-1}} + 4nk$
Acceptance ratio	Proposition 1	$T_{\mathbf{A}} + T_{\mathbf{L}} + 2n(k + 2)$

Table 1: Summary of computational costs of various steps in LRIS.

**A.** This is useful for applications in which  $T_{\mathbf{A}}$  can be extremely high. The computational cost of computing the acceptance ratio can be examined in light of Proposition 1. On each iteration, the weight  $w(\mathbf{x})$  will already be available from the previous iteration, so we only need to compute  $w(\mathbf{z})$ . We can simplify this expression as  $\log w(\mathbf{z}) = -\mu \mathbf{z}^\top (\mathbf{A}^\top \mathbf{A} - \mathbf{L}^\top \mathbf{V}_k \mathbf{\Lambda}_k \mathbf{V}_k^\top \mathbf{L}) \mathbf{z}$ , which requires one matvec with  $\mathbf{A}$  and  $\mathbf{L}$  each, two inner products and  $4n$  flops, and an additional  $2nk$  flops. Aside from the precomputational cost of the low-rank factorization, only the evaluation of the acceptance ratio requires accessing the forward operator  $\mathbf{A}$ . The resulting costs are summarized in Table 1.

## 4 Illustrations

Here we demonstrate our proposed approach on two simulated examples. The first example is a standard two dimensional deblurring problem in which we compare the performance of our proposed low-rank independence sampler to conventional block Gibbs sampling and deterministic MAP estimation to demonstrate the competitive solutions and the ability to access the entire posterior distribution in an efficient manner. The second example is a more challenging application motivated by medical imaging. We apply our proposed approach there to demonstrate feasibility and to consider a different prior on the precisions than the conventional independent conjugate Gammas.

To ensure meaningful inferences based on the MCMC output, it is important to assess whether the Markov chain is sufficiently close to its stationary distribution. It is well known that an MCMC procedure will generally not result in an immediate draw from the target distribution, unless the initial distribution is the stationary distribution. Usually it is not possible to prove that a chain has converged to its limiting distribution, except in special cases (e.g., perfect sampling [50, 17] or partially identified Gaussian linear models [20]). However, diagnostic tools can be used to assess whether or not a chain is sufficiently close so that one can safely treat its output as draws from the target distribution. To assess convergence, we use (scalar and multivariate) potential scale reduction factors (PSRF/MPSRF) [26, 11], trace plots, and autocorrelation plots as diagnostic tools. The reader is referred to [53, Ch. 12], [15, Ch. 3], or [24, Ch. 11] for further discussions of convergence diagnostics for MCMC.

### 4.1 2D Image Deblurring

We take as our target image a  $50 \times 50$  pixel grayscale image of geometric shapes so that  $n = 2500$  in (3). We blur the image by convolution with a Gaussian point spread function. The forward model  $\mathbf{A}$  and true image  $\mathbf{x}$  are created using the **Regularization Tools** package [29]. The data are generated by adding Gaussian noise with variance  $0.01^2 \|\mathbf{A}\mathbf{x}\|_\infty^2$ . Figure 1 displays the target image and the noisy data.

We model smoothness on  $\mathbf{x}$  *a priori* by taking  $\mathbf{L} = -\Delta + \delta \mathbf{I}$  in (3), where  $-\Delta$  is the discrete Laplacian and  $\delta$  is a small constant to ensure positive definiteness [37]. For the prior and noise precision parameters, we assign a vague Gamma prior,  $\text{Gamma}(0.1, 0.1)$ , which approximates the scale invariant objective prior while maintaining conditional conjugacy. (Details of implementation are given in [6].) We compute the eigenvalues of the prior preconditioned Hessian matrix  $\mathbf{H}$  via SVD (implemented using MATLAB’s `svds` command) to determine an appropriate cutoff. Figure 7 (dis-

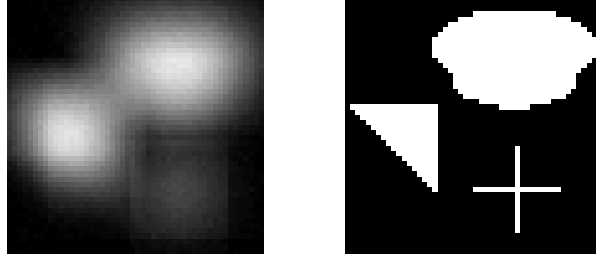


Figure 1: Blurred and noisy image (left panel) and true image (right panel) in the 2D image deblurring example.

cussed further below) indicates rapid decay within the first few eigenvalues, followed by a smoother decay, and another sharp decay. We use the first  $k = 500$  eigenvalues of the matrix to construct our low-rank approximation. We analyze below the effect of truncation level on the acceptance rate of the sampling algorithm. For comparison, we also compute a low-rank approximation using the Randomized SVD approach described in Section 3. To ensure the same number  $\ell = k + p$  of eigenvalues are retained with this approach, we specify a cutoff of  $k = 480$  and an oversampling parameter  $p = 20$ .

**Convergence and UQ metrics** We implement a Metropolis-Hastings-within-Gibbs algorithm in which Step 3 of Algorithm 1 is substituted with our proposed LRIS presented in Section 3. Three different chains are run in parallel, with each chain initialized by drawing  $\mathbf{x}$ ,  $\mu$ , and  $\sigma$  randomly from their prior distributions. Each chain is run for  $N = 50,000$  iterations with the first 25,000 iterations discarded as a burn-in period. We compare LRIS to the standard block Gibbs sampler for illustration. The Gibbs sampler is implemented identically to the low-rank procedure with three independent chains run in parallel with widely dispersed initial values. All simulations are done in MATLAB running on OS X Yosemite (8GB RAM, Intel Core i5 2.66GHz processor).

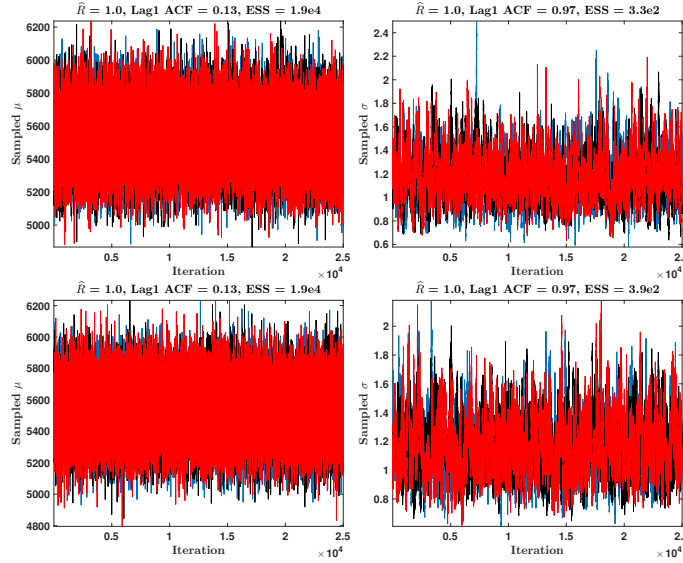


Figure 2: Trace plots of  $\mu$  (left) and  $\sigma$  (right) obtained from the MCMC output of both block Gibbs sampling (top row) and our proposed LRIS (bottom row), where each of the three colors represents a different chain. The potential scale reduction factors ( $\hat{R}$ ) are displayed above each plot, along with the lag 1 autocorrelation coefficients and effective sample size (ESS) estimated from one chain each under both approaches.

Figures 2 and 3 display trace plots and autocorrelation functions, respectively, for the last 25,000 iterations of the  $\mu$  and  $\sigma$  chains for both ordinary block Gibbs sampling and our proposed algorithm. As is known to occur with block Gibbs sampling in high-dimensional linear inverse problems [6], we observe near independence of the  $\mu$  chains and strong autocorrelation in the  $\sigma$  chains. Despite the high autocorrelation, we still are able to achieve approximate convergence and a sufficient effective sample size (ESS) from the  $\sigma$  chains by running each chain long enough. By combining the three independent chains after approximate convergence, we effectively triple the ESS and thus the number of independent pieces of information available about the target posterior. Thinning the chains to, e.g., every 10th, 50th, or 100th draw would dramatically reduce the autocorrelation of the chains. However, it was argued by Carlin and Louis [15] that such thinning is not necessary and does not improve estimates of quantities of interest. Indeed, Figure 4 illustrates the approximate convergence of the ergodic averages  $\hat{\mu}_{(n)} = n^{-1} \sum_{t=1}^n \mu_{(t)}$  and  $\hat{\sigma}_{(n)} = n^{-1} \sum_{t=1}^n \sigma_{(t)}$ ,  $n = 1, \dots, 25000$ , despite the high autocorrelation of the  $\sigma$  chain. The limiting values from both approaches closely agree, as expected.

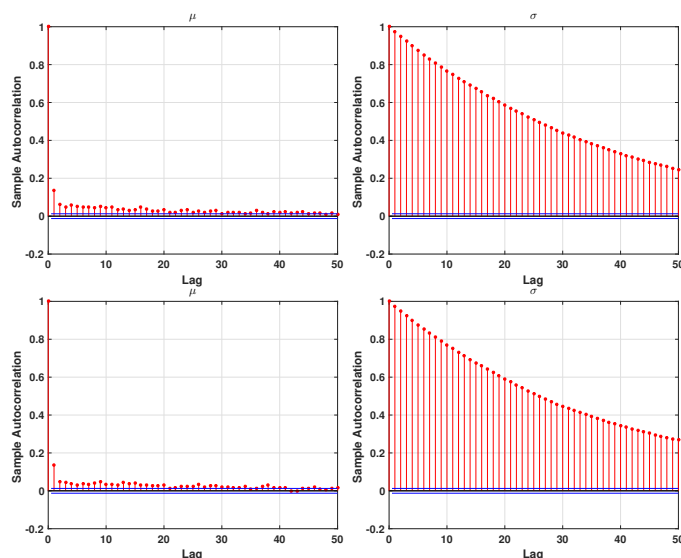


Figure 3: Autocorrelation functions of  $\mu$  (left) and  $\sigma$  (right) obtained from one of the chains each under block Gibbs sampling (top row) and our proposed low-rank independence sampling algorithm (bottom row).

While assessing convergence of high-dimensional parameters is more difficult than for scalar quantities, we can track realized values of the data-misfit part of the log-likelihood as a proxy for monitoring convergence. These realizations also should settle down as the chain approaches the target distribution. Figure 4 displays these plots for both algorithms along with the multivariate PSRFs. Again, we see consistency between ordinary block Gibbs and our own approach, as well as approximate convergence according to the rule of thumb that the PSRF should be less than or equal to approximately 1.1 [24].

The advantage of our proposed approach is clear in Table 4.1, which displays the total wall time to complete the 50,000 MCMC iterations for both block Gibbs and our proposed low-rank sampling approach. Table 4.1 also displays the *cost per effective sample* (CES) for one of the  $\sigma$  chains obtained under both algorithms as well as the Randomized SVD approach. CES is simply a measure of the average computational effort required between effectively independent draws. LRIS yields a 76% reduction in computation time compared to the standard block Gibbs sampler, along with an approximate 80% reduction in computational effort between independent draws of  $\sigma$ . The average acceptance rate over the three chains using our low-rank proposals is 98%, for both “exact” and Randomized SVD. The acceptance rate versus rank is discussed further below.

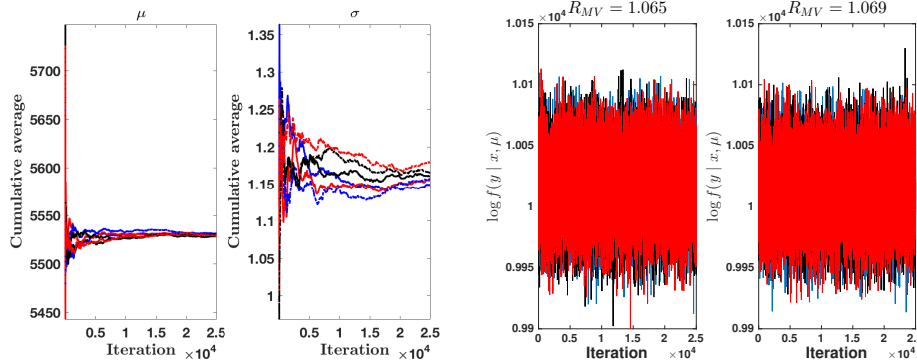


Figure 4: Cumulative averages of the  $\mu$  chains (far left) and  $\sigma$  chains (middle left) obtained from the MCMC output. The dotted lines represent the three chains from block Gibbs, the solid lines correspond to the low-rank algorithm output. Plot of the data-misfit part of the log-likelihood values calculated from the MCMC output of both block Gibbs sampling (middle right) and our low-rank independence sampling algorithm (far right), where each of the three colors corresponds to a different chain. The multivariate potential scale reduction factors are displayed above.

	Wall Time (s)	CES for $\sigma$
Block Gibbs	27907	84.3
Low-Rank Sampler	5134	13.20
Low-Rank Sampler (Randomized SVD)	5307	13.86

Table 2: Total wall time to complete 50,000 MCMC iterations under block Gibbs sampling and LRIS for the 2D deblurring example, along with the estimated cost per effective sample (CES) for one of the  $\sigma$  chains in each case.

We attain this dramatic reduction in computational effort without sacrificing the quality of posterior inferences, as evident in Figure 5. This Figure displays the approximate posterior means of  $\mathbf{x}$  from both block Gibbs and our low-rank approach. The estimators we obtain with Randomized SVD are similar and hence omitted. For completeness, we show also the  $(\mu, \sigma)$  scatterplots and approximate marginal densities obtained from both algorithms in Figure 6, again showing agreement between the two approaches. The strong Bayesian learning that occurred about these parameters is evident in Supplementary Figure 4. Table 3 displays the relative errors to quantify the quality of the reconstructions. We observe nearly identical solutions under both MCMC approaches, both graphically and quantitatively.

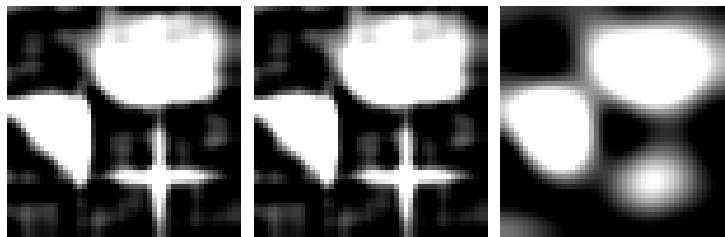


Figure 5: Approximate posterior mean images obtained from block Gibbs sampling (left panel) and the proposed low-rank sampling algorithm (middle panel) for the 2D deblurring example. The posterior mode (MAP) is also displayed in the right panel.

In addition to posterior means, we consider also the posterior mode (MAP), a common point estimator that corresponds to deterministic minimization of the objective function. The MAP estimate, obtained with a block coordinate descent on the negative log-likelihood of the joint posterior

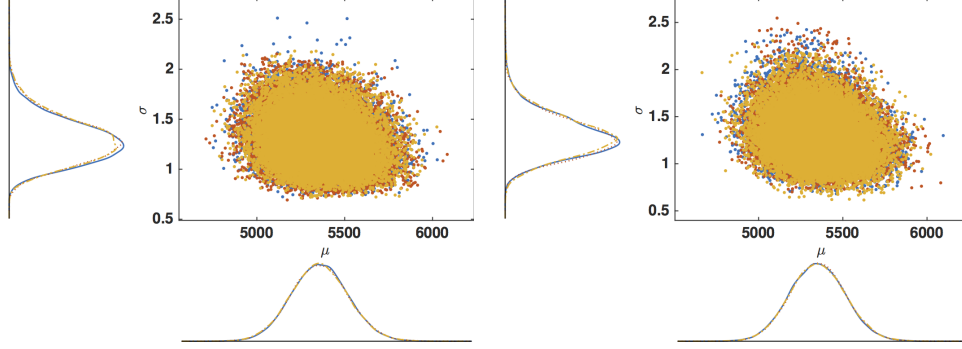


Figure 6: Scatter plots of the  $(\mu, \sigma)$  realizations obtained from block Gibbs (left panel) and the low-rank approach (right panel) for the 2D deblurring example, where the three different colors correspond to different chains. The smoothed marginal posterior densities are displayed in the margins of the plots.

Estimator	RE
Posterior Mean (Block Gibbs)	0.4453
Posterior Mean (Low-Rank)	0.4455
MAP	0.5285

Table 3: Relative error (RE) of the estimates for the 2D image deblurring example.

distribution, is displayed in Figure 5 and the reconstruction error quantified in Table 3. In this case, the posterior mean produces a more faithful reconstruction of the solution than the MAP, which is clearly overly smooth. This is not surprising, since the posterior mean is the Bayes estimator under squared-error loss (the most common loss function for estimation) [39, Ch. 4]. This is one reason why Carvalho et al. [16] argue in favor of the posterior mean for point estimation instead of the mode.

**Acceptance rate versus rank** To explore the effect of the retained number of eigenvalues on the acceptance rate for our algorithm, we estimate the predicted and empirical acceptance rates of sampling from the proposal distribution, over a range of truncation levels, at a given state of the chain. We fix the state by initializing  $(\mathbf{x}, \mu, \sigma)$  as the last sample from one of the chains obtained from LRIS. At each truncation level  $K$ , we compute the expected value of the acceptance ratio using Theorem 1. We draw 2,000 samples from the proposal distribution and compute the acceptance ratio of each using Proposition 2. From these we estimate the empirical failure rates to compare with their expected values as the truncation level increases. The results are displayed in Figure 7. The close agreement between the predicted and empirical acceptance rates support the theoretical results in Section 3.

## 4.2 CT Image Reconstruction

Computed x-ray tomography (CT) is a common medical imaging modality in which x-rays are passed through a body from a source to a sensor along parallel lines indexed by an angle  $\omega$  and offset  $y$  with respect to a fixed coordinate system and origin. The intensities of the rays are attenuated according to an unknown absorption function as they pass through tissue. The attenuated intensity  $I$  is recorded while the lines are rotated around the origin so that  $I(S) = I(0) \exp\{-\int_0^S \alpha(x(s)) ds\}$ , where  $s = 0$  is the source of the x-ray,  $s = S$  is the receiver location,  $x(\cdot)$  indicates the line position, and  $\alpha$  is the absorption function. The observed data are a transformation of the intensities, yielding the Radon transform model for CT [37, 5],  $z(\omega, y) = \int_{L(\omega, y)} \alpha(x(s)) ds$ , where  $L(\omega, y)$  is the line along which the x-ray passes through the body. The inverse problem is to reconstruct the absorption

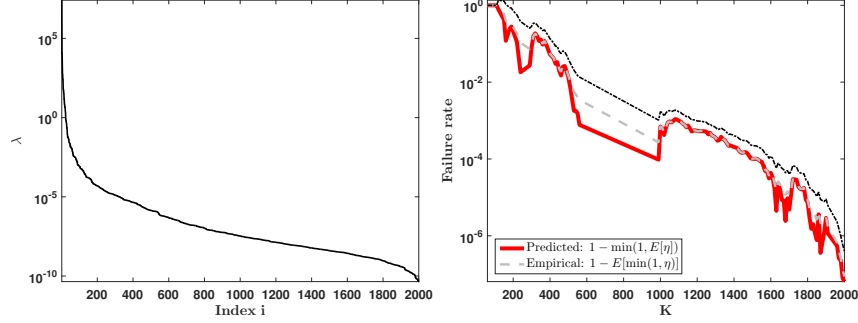


Figure 7: (left) Eigenvalues of  $\mathbf{H}$  in the 2D image deblurring example. (right) Predicted and empirical failure rates for different truncation levels  $K$ . The empirically determined upper 0.975 quantile is given by the dashed line; the lower quantile often attained zero values, so it is not displayed.

function, which provides an image of the scanned body. Discretization of the integral yields the model in (1). This is typically an underdetermined system with infinitely many solutions, resulting in an ill-posed inverse problem.

Our target image is the Shepp-Logan phantom [62]. The forward model is implemented in MATLAB on the same system as in Section 4.1 with code available online [4]. The data are simulated by adding Gaussian noise with variance  $0.01^2 \|\mathbf{Ax}\|_\infty^2$ . The target  $\alpha$  is discretized to a relatively fine grid of size  $128 \times 128$  so that  $\dim(\mathbf{x}) = 16,384$ . We suppose that the data are observed over lines and angles such that  $\dim(\mathbf{b}) = 5000$ . Thus,  $\text{rank}(\mathbf{A}) = 5000 \ll \dim(\mathbf{x})$ , guiding our choice of eigenvalue truncation in the low-rank approximation to  $\mathbf{H}$ . An approximate eigendecomposition of the prior preconditioned Hessian is computed using Randomized SVD with target rank 4900, as discussed in Section 3, since computing the “exact” SVD is considerably more expensive. As in Section 4.1, we take  $\mathbf{L} = -\Delta + \delta \mathbf{I}$ .

For the nuisance parameters, we use a weakly informative prior [23], namely the proper Jeffreys prior proposed by Scott and Berger [61]. For convenience, we parameterize the model in terms of variance components instead of precisions,  $\tau^2 := \sigma^{-1}$  and  $\kappa^2 := \mu^{-1}$ . Then the proper Jeffreys prior on  $(\kappa^2, \tau^2)$  is<sup>2</sup>

$$\begin{aligned} \pi_{SB}(\kappa^2, \tau^2) &= (\kappa^2 + \tau^2)^{-2} \\ &= (\kappa^2)^{-1} (1 + \tau^2/\kappa^2)^{-2} \times (\kappa^2)^{-1} \\ &\equiv \pi(\tau^2 | \kappa^2) \pi(\kappa^2), \end{aligned} \tag{17}$$

so that the scale invariant prior is used for  $\kappa^2$  while scaling  $\tau^2$  by the data level variance, as advocated by Jeffreys [35]. The implementation of this prior as a modification to Algorithm 1, presented in Appendix B, is similar to the approach of [12]. Section 1 of the Supplementary Material contains further discussion of prior specification for the nuisance parameters.

We simulate three Markov chains using our proposed low-rank proposal for 40,000 iterations (average acceptance rate  $\sim 100\%$ ). Each chain is initialized with values drawn randomly from the prior. We thin the chains by retaining every 50th draw to reduce the autocorrelation, making it easier to diagnose convergence. We discard the first 400 draws of the thinned chains as a burn-in period. Trace plots and autocorrelation plots are used to verify approximate convergence of the chains. Relevant diagnostic plots are displayed in Figures 5, 6, and ?? in the Supplementary Material. The total computation time for our sampling approach is 197,517 seconds, or about 55 hours. This is noteworthy since the algorithm repeatedly updates a large, nontrivial covariance matrix and samples an approximately sixteen-thousand dimensional Gaussian distribution 40,000 times.

<sup>2</sup>We write ‘proportional to’ ( $\pi(\theta) \propto g(\theta)$ ) for proper priors to indicate that  $\pi(\theta) = cg(\theta)$ , where  $c^{-1} = \int g(\theta)d\theta < \infty$  uniquely determines the density. However, the normalizing constant for an improper prior does not exist, so there is no normalizing constant to uniquely determine it. In the scale invariant case, any prior  $\pi(\kappa^2) = c/\kappa^2$  for  $c \neq 0$  works. Since  $c$  is arbitrary, we simply set it equal to 1 for convenience and take  $\pi(\kappa^2) = 1/\kappa^2$ . See [10, Chapter 3].

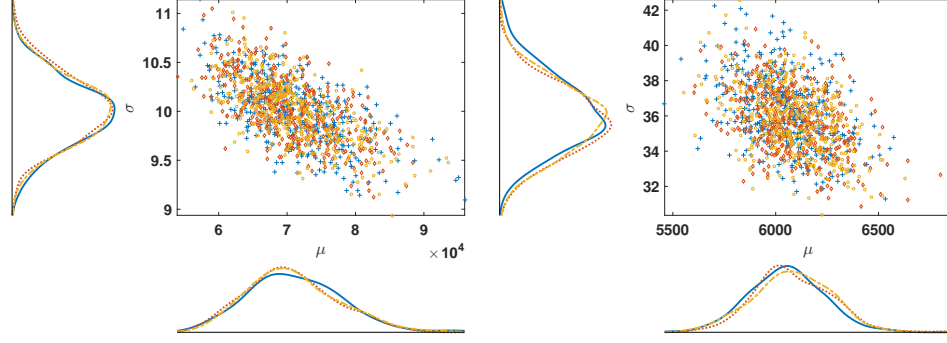


Figure 8: Estimated joint densities for the precision parameters using the proper Jeffreys prior (left) and the conjugate Gamma priors (right).

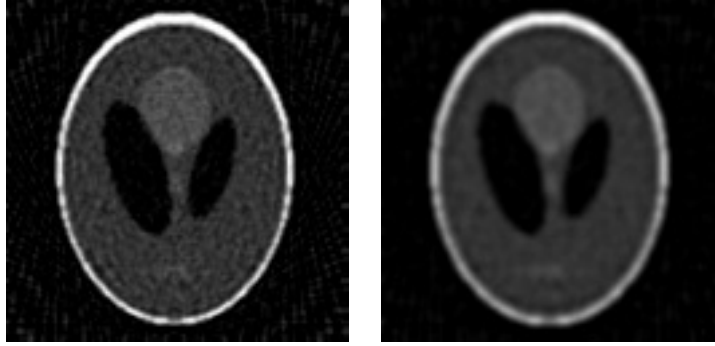


Figure 9: Posterior mean estimators of the true image in the CT image reconstruction example, using the proper Jeffreys prior (left) and the conjugate Gamma priors (right).

Lastly, we compare the results with samples obtained using the conjugate Gamma model with the same vague priors on  $\mu$  and  $\sigma$  as in Section 4.1. Convergence diagnostics are displayed in Supplementary Figures 8 and 9. Figure 8 compares the approximate joint distributions for the precision parameters  $(\mu, \sigma)$  under the conjugate model to the distribution based on the proper Jeffreys model, after back-transforming  $\kappa^2$  and  $\tau^2$ . Here we see the effect of prior selection in that both  $\mu$  and  $\sigma$  tend to concentrate around different values, with much greater uncertainty in  $\mu$  in the proper Jeffreys case. The differences between the two marginal posteriors of  $(\mu, \sigma)$  affect the quality of the reconstructed images, displayed in Figure 9 and quantified in Table 4. This echoes Gelman’s observation [23] that even a supposedly noninformative prior on the hyper-precision can have a disproportionate influence on the results. In this case, using a weakly informative prior for  $\sigma$  that depends on  $\mu$  results in a higher quality reconstruction.

Posterior Mean	RE
Proper Jeffreys	0.3270
Conjugate Gamma	0.4229

Table 4: Relative error (RE) of the estimates for the CT image reconstruction example.

These simulations show that by exploiting the low-rank structure of the preconditioned Hessian of the forward model, we are able to substantially reduce the computational burden compared to block Gibbs sampling. Even when the forward model is of full row rank, the results illustrate the potential for efficiency gains using our proposed LRIS approach, provided the system is underdetermined. Our approach using either proper Jeffreys or conjugate priors is much more feasible than a block Gibbs sampler, for which the computational demands can be prohibitively expensive. A comparison of the conventional conjugate Gamma priors to a weakly informative prior suggests that even a

“noninformative” prior may exert considerable influence on the results, despite strong Bayesian learning in the posterior.

## 5 Discussion

When approximating the posterior distribution via Markov chain Monte Carlo in the Bayesian Gaussian linear inverse problem, the bottleneck is in repeatedly sampling high-dimensional Gaussian random variables. Repeatedly sampling from the joint posterior with standard block Gibbs is challenging due to the high dimensionality of the estimand, since drawing from the full conditional involves expensive operations with the covariance matrix. In this work we propose a computationally efficient sampling algorithm which is well suited for a fully Bayesian approach in which the noise precision and the prior precision parameters are unknown and assigned prior distributions. Our proposed low rank independence sampler uses a proposal distribution constructed via low-rank approximation to the preconditioned Hessian. We show that the acceptance rate is high when the magnitudes of the discarded eigenvalues of the Hessian are small, a feature of severely ill-posed problems. We demonstrate both theoretically and empirically that the quality of the approximation is directly related to the acceptance rate of the sampler, as intuition would suggest. We illustrate our approach on two examples, demonstrating computational improvements while also offering access to the full posterior distribution, thereby facilitating uncertainty quantification.

Our comparison of conventional conjugate Gamma priors on the nuisance parameters versus a more formally justified weakly informative prior shows that they can lead to substantially different marginal posterior distributions. This does not always have a dramatic effect on the reconstructed solution of interest [15], but our experiment did produce a noticeable difference in the reconstruction. While this is likely due to the fact that the proper Jeffreys prior scales the prior variance by the data level variance instead of treating them independently, the precise nature of how such priors behave in linear inverse problems is, as far as we know, not yet fully understood. This is possibly an interesting avenue for future research.

A known issue with block Gibbs sampling in Bayesian inverse problems is the deterioration of the chains due to correlation between the hyperparameters and the estimand  $\mathbf{x}$  as the dimension of the problem increases [6]. Several approaches have been proposed to ameliorate this by breaking the dependence between the hyperparameters and  $\mathbf{x}$  in the algorithm. These include the one-block algorithm [55], partially collapsed samplers [67, 8], noncentered parameterization (NCP) [46, 47], and marginal then conditional (MTC) sampling [19]. Noncentered parameterization is easily incorporated into our proposed approach without sacrificing gains in efficiency. (See the Supplementary Material for discussion of NCP and illustration of combining it with our low-rank sampler.) One-block sampling and MTC, on the other hand, require expressions for marginal densities that no longer hold when substituting the true full conditional of  $\mathbf{x}$  with an approximation, as well as approximation of determinants of large covariance matrices to which the results in this work are not directly applicable. Combining our proposed low-rank sampling approach with these algorithms is the subject of ongoing research, to appear in future work.

## 6 Acknowledgements

This material is based upon work partially supported by the National Science Foundation under Grant DMS-1127914 to the Statistical and Applied Mathematical Sciences Institute (SAMSI). The authors thank the Editors, an Associate Editor, and two referees for comments and suggestions that improved this manuscript. The authors also would like to thank Duy Thai, Vered Madar, Johnathan Bardsley, and Ray Falk for useful conversations. Much of this work was done while the first author was a Visiting Research Fellow at SAMSI. DAB is partially supported by Grant CMMI-1563435 from the National Science Foundation.



## A Proofs

*Proof of Proposition 2:* The difference between the true and the approximate covariance matrices can be expressed as

$$\begin{aligned}\mathbf{\Gamma}_{\text{cond}}^{-1} - \widehat{\mathbf{\Gamma}}_{\text{cond}}^{-1} &= \mu \mathbf{A}^\top \mathbf{A} + \sigma \mathbf{L}^\top \mathbf{L} - \left( \mu \mathbf{L}^\top \mathbf{V}_k \mathbf{\Lambda}_k \mathbf{V}_k \mathbf{L} + \sigma \mathbf{L}^\top \mathbf{L} \right), \\ &= \mu \mathbf{L}^\top \left( \mathbf{L}^{-\top} \mathbf{A}^\top \mathbf{A} \mathbf{L}^{-1} - \mathbf{V}_k \mathbf{\Lambda}_k \mathbf{V}_k \right) \mathbf{L}, \\ &= \mu \mathbf{L}^\top \left( \sum_{j=k+1}^n \lambda_j \mathbf{v}_j \mathbf{v}_j^\top \right) \mathbf{L},\end{aligned}$$

giving that  $\log w(\mathbf{x}) = -\frac{\mu}{2} \sum_{j=k+1}^n \lambda_j (\mathbf{v}_j^\top \mathbf{L} \mathbf{x})^2 \leq 0$ , and hence the acceptance ratio is given by (12).  $\square$

**Lemma 1.** *Suppose  $\mathbf{M}$  is symmetric positive definite. Then,*

$$\int_{\mathbb{R}^n} \exp \left( -\frac{1}{2} \mathbf{z}^\top \mathbf{M} \mathbf{z} + \mathbf{J}^\top \mathbf{z} \right) d\mathbf{z} = \frac{(2\pi)^{n/2}}{\det(\mathbf{M})^{1/2}} \exp \left( \frac{1}{2} \mathbf{J}^\top \mathbf{M}^{-1} \mathbf{J} \right).$$

*Proof.* See [60, Lemma B.1.1].  $\square$

**Lemma 2.** *The moments of the acceptance ratio are*

$$\mathbb{E}_{\mathbf{z}|\mathbf{x}}[\eta^m(\mathbf{z}, \mathbf{x})] = \frac{1}{N_m w^m(\mathbf{x})},$$

where  $N_m$  is defined in (13).

*Proof.* The proof proceeds in four steps.

1. *Simplifying  $\mathbb{E}_{\mathbf{z}|\mathbf{x}}[w^m(\mathbf{z})]$ .* We focus on  $\mathbb{E}_{\mathbf{z}|\mathbf{x}}[w^m(\mathbf{z})]$ . By definition, this is

$$\int_{\mathbb{R}^n} w^m(\mathbf{z}) g(\mathbf{z}) d\mathbf{z} = \frac{\exp \left( -\frac{1}{2} (\hat{\mathbf{x}}_{\text{cond}})^\top \widehat{\mathbf{\Gamma}}_{\text{cond}}^{-1} \hat{\mathbf{x}}_{\text{cond}} \right)}{(2\pi)^{n/2} \det(\widehat{\mathbf{\Gamma}}_{\text{cond}})^{1/2}} \int \exp \left( -\frac{1}{2} \mathbf{z}^\top \mathbf{M} \mathbf{z} + \mathbf{J}^\top \mathbf{z} \right) d\mathbf{z},$$

where, by using  $\hat{\mathbf{x}}_{\text{cond}} = \mu \widehat{\mathbf{\Gamma}}_{\text{cond}} \mathbf{A}^\top \mathbf{b}$ , we get,

$$\mathbf{M} = m(\mathbf{\Gamma}_{\text{cond}}^{-1} - \widehat{\mathbf{\Gamma}}_{\text{cond}}^{-1}) + \widehat{\mathbf{\Gamma}}_{\text{cond}}^{-1}, \quad \text{and} \quad \mathbf{J} = \widehat{\mathbf{\Gamma}}_{\text{cond}}^{-1} \hat{\mathbf{x}}_{\text{cond}} = \mu \mathbf{A}^\top \mathbf{b}.$$

Applying Lemma 1 and rearranging, we have

$$\mathbb{E}_{\mathbf{z}|\mathbf{x}}[w^m(\mathbf{z})] = \frac{\exp \left( \frac{\mu^2}{2} (\mathbf{A}^\top \mathbf{b})^\top (\mathbf{M}^{-1} - \widehat{\mathbf{\Gamma}}_{\text{cond}}) \mathbf{A}^\top \mathbf{b} \right)}{\det(\mathbf{M})^{1/2} \det(\widehat{\mathbf{\Gamma}}_{\text{cond}})^{1/2}}. \quad (18)$$

We focus on the numerator and denominator of (18) separately.

2. *Denominator of (18).* Note that

$$\mathbf{M} = m(\mathbf{\Gamma}_{\text{cond}}^{-1} - \widehat{\mathbf{\Gamma}}_{\text{cond}}^{-1}) + \widehat{\mathbf{\Gamma}}_{\text{cond}}^{-1} = m\mathbf{\Gamma}_{\text{cond}}^{-1} + (1-m)\widehat{\mathbf{\Gamma}}_{\text{cond}}^{-1}$$

and furthermore,

$$\mathbf{M} = \mathbf{L}^\top \left( \mu \sum_{j=1}^k \lambda_j \mathbf{v}_j \mathbf{v}_j^\top + m\mu \sum_{j=k+1}^n \lambda_j \mathbf{v}_j \mathbf{v}_j^\top + \sigma \mathbf{I} \right) \mathbf{L}.$$

Using the properties of determinants, it can be shown that

$$\det(\mathbf{M}) = \sigma^n \det(\mathbf{L})^2 \prod_{j=1}^k \left(1 + \frac{\mu}{\sigma} \lambda_j\right) \prod_{j=k+1}^n \left(1 + \frac{m\mu}{\sigma} \lambda_j\right).$$

Similarly,

$$\det(\widehat{\mathbf{\Gamma}}_{\text{cond}}^{-1}) = \sigma^n \det(\mathbf{L})^2 \prod_{j=1}^k \left(1 + \frac{\mu}{\sigma} \lambda_j\right).$$

Combining these results, the denominator of (18) becomes

$$\det(\mathbf{M})^{1/2} \det(\widehat{\mathbf{\Gamma}}_{\text{cond}})^{1/2} = \sqrt{\frac{\det(\mathbf{M})}{\det(\widehat{\mathbf{\Gamma}}_{\text{cond}})}} = \prod_{j>k} \left(1 + \frac{m\mu}{\sigma} \lambda_j\right)^{1/2}.$$

3. *Numerator of (18).* Consider  $\mathbf{M}^{-1} - \widehat{\mathbf{\Gamma}}_{\text{cond}}$ . By the Woodbury matrix identity,

$$\begin{aligned} \mathbf{M}^{-1} - \widehat{\mathbf{\Gamma}}_{\text{cond}} &= \left(m\mathbf{\Gamma}_{\text{cond}}^{-1} + (1-m)\widehat{\mathbf{\Gamma}}_{\text{cond}}^{-1}\right)^{-1} - \widehat{\mathbf{\Gamma}}_{\text{cond}} \\ &= \frac{1}{\sigma} \mathbf{L}^{-1} \left( \mathbf{I} - \sum_{j=1}^k \frac{\mu \lambda_j}{\mu \lambda_j + \sigma} \mathbf{v}_j \mathbf{v}_j^\top - \sum_{j=k+1}^n \frac{m\mu \lambda_j}{m\mu \lambda_j + \sigma} \mathbf{v}_j \mathbf{v}_j^\top \right) \mathbf{L}^{-\top} \\ &\quad - \frac{1}{\sigma} \left( \mathbf{I} - \sum_{j=1}^k \frac{\mu \lambda_j}{\mu \lambda_j + \sigma} \mathbf{v}_j \mathbf{v}_j^\top \right) \mathbf{L}^{-\top} \\ &= -\frac{1}{\sigma} \sum_{j=k+1}^n \frac{m\mu \lambda_j}{m\mu \lambda_j + \sigma} \mathbf{L}^{-1} \mathbf{v}_j \mathbf{v}_j^\top \mathbf{L}^{-\top}. \end{aligned}$$

The numerator is therefore,

$$\exp \left( \frac{\mu^2}{2} (\mathbf{A}^\top \mathbf{b})^\top (\mathbf{M}^{-1} - \widehat{\mathbf{\Gamma}}_{\text{cond}}) \mathbf{A}^\top \mathbf{b} \right) = \exp \left( -\frac{\mu^2}{2\sigma} \sum_{j=k+1}^n \frac{m\mu \lambda_j}{m\mu \lambda_j + \sigma} (\mathbf{b}^\top \mathbf{A} \mathbf{L}^{-1} \mathbf{v}_j)^2 \right).$$

4. *Combining intermediate results.* Plugging the results of Steps 2 and 3 into (18), gives us  $\mathbb{E}_{\mathbf{z}|\mathbf{x}}[w^m(\mathbf{z})] = \frac{1}{N_m}$ , where  $N_m$  is defined in (13). The proof readily follows because  $\mathbb{E}_{\mathbf{z}|\mathbf{x}}[\eta^m(\mathbf{z}, \mathbf{x})] = \mathbb{E}_{\mathbf{z}|\mathbf{x}}[w^m(\mathbf{z})]/w^m(\mathbf{x})$ .  $\square$

*Proof of Theorem 1:* From Lemma 2, we have  $\mathbb{E}_{\mathbf{z}|\mathbf{x}}[\eta^m(\mathbf{z}, \mathbf{x})] = \frac{1}{N_m w^m(\mathbf{x})}$ . The first result follows immediately by plugging in  $m = 1$ . For the second result observe that for a random variable  $X$ ,  $\mathbb{V}[X] = \mathbb{E}[(X - \mathbb{E}[X])^2] = \mathbb{E}[X^2] - (\mathbb{E}[X])^2$ . The result follows from (14) and applying Lemma 2 with  $m = 2$ .  $\square$

*Proof of Proposition 3:* Using  $h$  as defined in (11) and the definition of the proposal density  $g$ ,

$$\frac{h(\mathbf{x})}{g(\mathbf{x})} = \sqrt{\frac{\det(\widehat{\mathbf{\Gamma}}_{\text{cond}})}{\det(\mathbf{\Gamma}_{\text{cond}})}} w(\mathbf{x}) \exp \left( -\frac{\mu^2}{2} \mathbf{b}^\top \mathbf{A} (\mathbf{\Gamma}_{\text{cond}} - \widehat{\mathbf{\Gamma}}_{\text{cond}}) \mathbf{A}^\top \mathbf{b} \right).$$

From the proof of Lemma 2,  $\mathbf{M}^{-1} = \mathbf{\Gamma}_{\text{cond}}$  when  $m = 1$ . Comparing terms with (18) this gives us  $h(\mathbf{x}) = N_1 g(\mathbf{x}) w(\mathbf{x})$ , where  $N_1$  is defined in (13). From the proof of Proposition 2,  $\log w(\mathbf{x}) \leq 0$ , and therefore  $w(\mathbf{x}) \leq 1$ . The desired result follows. Note that the bound is tight because  $w(\mathbf{0}) = 1$ .  $\square$

*Proof of Theorem 2:* It is easy to show that  $w(\mathbf{x}) \leq 1$ , therefore,  $\eta(\mathbf{z}, \mathbf{x}) \geq w(\mathbf{z})$ . From Proposition 1, we need to consider the quadratic form

$$\frac{1}{2} \mathbf{z}^\top (\mathbf{\Gamma}_{\text{cond}}^{-1} - \widehat{\mathbf{\Gamma}}_{\text{cond}}^{-1}) \mathbf{z} = \frac{\mu}{2} \mathbf{z}^\top \mathbf{L}^\top (\mathbf{H} - \widehat{\mathbf{H}}) \mathbf{L} \mathbf{z},$$

where  $\widehat{\mathbf{H}}$  is the low-rank approximation. This follows from  $\widehat{\mathbf{\Gamma}}_{\text{cond}}^{-1} = (\mu \mathbf{L}^\top \widehat{\mathbf{H}} \mathbf{L} + \sigma \mathbf{L}^\top \mathbf{L})$ . Using Cauchy-Schwartz inequality, we can bound (in the spectral norm)

$$\mathbf{z}^\top \mathbf{L}^\top (\mathbf{H} - \widehat{\mathbf{H}}) \mathbf{L} \mathbf{z} \leq \|\mathbf{L} \mathbf{z}\|^2 \|\mathbf{H} - \widehat{\mathbf{H}}\|.$$

Arguing as in [28, Section 5.3], we have  $\|\mathbf{H} - \widehat{\mathbf{H}}\| \leq 2\|\mathbf{H} - \mathbf{Q} \mathbf{Q}^\top \mathbf{H}\|$ . Applying [28, Theorem 10.6] we have

$$\mathbb{E}_{\Omega} \|\mathbf{H} - \widehat{\mathbf{H}}\| \leq 2 \left[ \alpha \lambda_{k+1} + \beta \left( \sum_{j=k+1}^n \lambda_j^2 \right)^{1/2} \right], \quad (19)$$

with constants  $\alpha$  and  $\beta$  given in the statement of the result. Applying Jensen's inequality

$$\mathbb{E}_{\Omega} [\eta(\mathbf{z}, \mathbf{x})] \geq \exp \left( -\mu \|\mathbf{L} \mathbf{z}\|^2 \mathbb{E}_{\Omega} \|\mathbf{H} - \widehat{\mathbf{H}}\| \right).$$

Plug in (19) into the above equation to complete the proof.  $\square$

## B Implementing the Proper Jeffreys Prior

Here we briefly discuss an implementation of the LRIS algorithm when the Scott-Berger prior (17) is used instead of the independent conjugate Gamma priors.

In this case, the model (17) becomes

$$\begin{aligned} \mathbf{y} \mid \mathbf{x}, \kappa^2 &\sim N(\mathbf{A} \mathbf{x}, \kappa^2 \mathbf{I}) \\ \mathbf{x} \mid \tau^2 &\sim N(\mathbf{0}, \tau^2 \mathbf{\Gamma}) \\ \pi(\tau^2 \mid \kappa^2) &\propto \kappa^{-2} (1 + \tau^2 / \kappa^2)^{-2} \\ \pi(\kappa^2) &\propto \kappa^{-2}. \end{aligned} \quad (20)$$

To obtain the full conditional densities necessary for Gibbs sampling, it is convenient to reparameterize the model with  $v = \tau^2 / \kappa^2$ . After the change of variables, the joint posterior (5) becomes

$$\begin{aligned} \pi(\mathbf{x}, \kappa^2, v \mid \mathbf{b}) &\propto (\kappa^2)^{-\frac{m+n}{2}-1} v^{-n/2} (1+v)^{-2} \\ &\times \exp \left( -\frac{1}{2\kappa^2} \left[ \|\mathbf{A} \mathbf{x} - \mathbf{b}\|_2^2 + \frac{1}{v} \|\mathbf{L} \mathbf{x}\|_2^2 \right] \right). \end{aligned} \quad (21)$$

The full conditional on  $\mathbf{x}$  is a standard result for the Normal-Normal model (4); i.e.

$$\mathbf{x} \mid \kappa^2, v, \mathbf{b} \sim \mathcal{N}(\mathbf{x}_{\text{cond}}, \mathbf{\Gamma}_{\text{cond}}),$$

where  $\mathbf{\Gamma}_{\text{cond}} = \kappa^2 \left( \mathbf{A}^\top \mathbf{A} + v^{-1} \mathbf{\Gamma}_{\text{pr}}^{-1} \right)^{-1}$  and  $\mathbf{x}_{\text{cond}} = \left( \mathbf{A}^\top \mathbf{A} + v^{-1} \mathbf{\Gamma}_{\text{pr}}^{-1} \right)^{-1} \mathbf{A}^\top \mathbf{b}$ . We can sample from this density using our proposed low-rank approximation approach. (See Section 3.) The full conditional on  $\kappa^2$  is

$$\kappa^2 \mid \mathbf{x}, v, \mathbf{y} \sim \text{InvGamma} \left( \frac{m+n}{2}, \frac{1}{2} \|\mathbf{A} \mathbf{x} - \mathbf{b}\|_2^2 + \frac{1}{2v} \|\mathbf{L} \mathbf{x}\|_2^2 \right).$$

To draw from this density, draw  $W \sim \text{Gamma}(\frac{m+n}{2}, \frac{1}{2}\|\mathbf{Ax} - \mathbf{b}\|_2^2 + \frac{1}{2v}\|\mathbf{Lx}\|_2^2)$  and set  $\kappa^2 = 1/W$ . The full conditional on  $v$  is

$$\pi(v \mid \mathbf{x}, \kappa^2, \mathbf{b}) \propto v^{-(n/2+1)-1} \exp\left[-\frac{1}{2\kappa^2 v}\|\mathbf{Lx}\|_2^2\right] \left(\frac{v}{1+v}\right)^2 \quad (22)$$

$$\equiv h(v) \left(\frac{v}{1+v}\right)^2, \quad (23)$$

where  $h(v)$  is the density of an  $\text{InvGamma}((n+2)/2, \|\mathbf{Lx}\|_2^2/(2\kappa^2))$  distribution. This density is not available directly. However, since

$$\frac{\pi(v \mid \mathbf{x}, \kappa^2, \mathbf{b})}{h(v)} = \left(\frac{v}{1+v}\right)^2 \leq 1 \quad \forall v,$$

we can use an independence Metropolis-Hastings algorithm with candidate distribution

$$\text{InvGamma}((n+2)/2, \|\mathbf{Lx}\|_2^2/(2\kappa^2))$$

to sample from the distribution with density  $h(v)$ .

## References

- [1] S. Agapiou, J. M. Bardsley, O. Papaspiliopoulos, and A. M. Stuart. Analysis of the Gibbs sampler for hierarchical inverse problems. *SIAM/ASA Journal on Uncertainty Quantification*, 2(1):511–544, 2014.
- [2] S. Ambikasaran, A. K. Saibaba, E. F. Darve, and P. K. Kitanidis. Fast algorithms for Bayesian inversion. In *Computational Challenges in the Geosciences*, pages 101–142. Springer, 2013.
- [3] K. E. Andersen, S. P. Brooks, and M. B. Hansen. Bayesian inversion of geoelectrical resistivity data. *J. R. Stat. Soc. Ser. B. Stat. Methodol.*, 65(3):619–642, 2003.
- [4] J. M. Bardsley. WMRNSD for medical imaging examples. <http://www.math.umd.edu/bardsley/codes.html>. Accessed: 2016-06-23.
- [5] J. M. Bardsley. Applications of nonnegatively constrained iterative method with statistically based stopping rules to CT, PET, and SPECT imaging. *Electron. Trans. Numer. Anal.*, 38:34–43, 2011.
- [6] J. M. Bardsley. MCMC-based image reconstruction with uncertainty quantification. *SIAM J. Sci. Comput.*, 34(3):A1316–A1332, 2012.
- [7] J. M. Bardsley, M. Howard, and J. G. Nagy. Efficient MCMC-based image deblurring with Neumann boundary conditions. *Electron. Trans. Numer. Anal.*, 40:476–488, 2013.
- [8] J. M. Bardsley, K. T. Joyce, and A. Luttman. Partially Collapsed Gibbs Samplers for Linear Inverse Problems and Applications to X-ray Imaging. *Manuscript in submission*, 2016.
- [9] J. M. Bardsley and A. Luttman. A Metropolis-Hastings method for linear inverse problems with Poisson likelihood and Gaussian prior. *Int. J. Uncertain. Quantif.*, 6(1):35–55, 2016.
- [10] J. O. Berger. *Statistical Decision Theory and Bayesian Analysis*. Springer-Verlag, New York, 2nd edition, 1985.
- [11] S. P. Brooks and A. Gelman. General methods for monitoring convergence of iterative simulations. *J. Comput. Graph. Statist.*, 7(4):434–455, 1998.
- [12] D. A. Brown, G. S. Datta, and N. A. Lazar. A Bayesian generalized CAR model for correlated signal detection. *Statistica Sinica*, 27:1125–1153, 2017.

- [13] T. Bui-Thanh, O. Ghattas, J. Martin, and G. Stadler. A computational framework for infinite-dimensional Bayesian inverse problems part i: The linearized case, with application to global seismic inversion. *SIAM J. Sci. Comput.*, 35(6):A2494–A2523, 2013.
- [14] D. Calvetti, J. P. Kaipio, and E. Somersalo. Inverse Problems in the Bayesian Framework. *Inverse Problems*, 30(11), 2014.
- [15] B. P. Carlin and T. A. Louis. *Bayesian Methods for Data Analysis*. Chapman & Hall/CRC, Boca Raton, 3rd edition, 2009.
- [16] C. M. Carvalho, N. G. Polson, and J. G. Scott. The horseshoe estimator for sparse signals. *Biometrika*, 97(2):465–480, 2010.
- [17] R. V. Craiu and X.-L. Meng. Perfection within reach: Exact MCMC sampling. In S. Brooks, A. Gelman, G. L. Jones, and X.-L. Meng, editors, *Handbook of Markov Chain Monte Carlo*, pages 199–226. Chapman & Hall/CRC Press, 2011.
- [18] H. P. Flath, L. C. Wilcox, V. Akçelik, J. Hill, B. van Bloemen Waanders, and O. Ghattas. Fast algorithms for Bayesian uncertainty quantification in large-scale linear inverse problems based on low-rank partial Hessian approximations. *SIAM J. Sci. Comput.*, 33(1):407–432, 2011.
- [19] C. Fox and R. A. Norton. Fast sampling in a linear–Gaussian inverse problem. *SIAM/ASA Journal on Uncertainty Quantification*, 4:1191–1218, 2016.
- [20] A. E. Gelfand and S. K. Sahu. Identifiability, improper priors, and Gibbs sampling for generalized linear models. *J. Am. Stat. Assoc.*, 94(445):247–253, 1999.
- [21] A E Gelfand, S K Sahu, and B P Carlin. Efficient parameterisations for normal linear mixed models. *Biometrika*, 82(3):479–488, 1995.
- [22] A. E. Gelfand and A. F. M. Smith. Sampling-based approaches to calculating marginal densities. *J. Am. Stat. Assoc.*, 85(410):398–409, 1990.
- [23] A. Gelman. Prior distributions for variance parameters in hierarchical models. *Bayesian Anal.*, 1(3):515–533, 2006.
- [24] A. Gelman, J. B. Carlin, H. S. Stern, D. B. Dunson, A. Vehtari, and D. B. Rubin. *Bayesian Data Analysis*. Chapman & Hall/CRC, Boca Raton, 3rd edition, 2014.
- [25] A. Gelman, G. Roberts, and W. Gilks. Efficient Metropolis jumping rules. In J. M. Bernardo, J. O. Berger, A. P. Dawid, and A. F. M. Smith, editors, *Bayesian Statistics 5*, volume 5, pages 599–607. Oxford University Press, New York, 1995.
- [26] A. Gelman and D. B. Rubin. Inference from iterative simulation using multiple sequences (with discussion). *Statist. Sci.*, 7:457–511, 1992.
- [27] S. Geman and D. Geman. Stochastic relaxation, Gibbs distributions and the Bayesian restoration of images. *IEEE Transactions on Pattern Analysis and Machine Intelligence*, 6:721–741, 1984.
- [28] N. Halko, P. G. Martinsson, and J. A. Tropp. Finding structure with randomness: Probabilistic algorithms for constructing approximate matrix decompositions. *SIAM rev.*, 53(2):217–288, 2011.
- [29] P. C. Hansen. Regularization tools version 4.0 for Matlab 7.3. *Numer. Algorithms*, 46:189–194, 2007.
- [30] P. C. Hansen. *Discrete inverse problems: insight and algorithms*, volume 7. SIAM, 2010.
- [31] W. Hastings. Monte Carlo sampling methods using Markov chains and their application. *Biometrika*, 57:97–109, 1970.

- [32] O. Hauk. Keep it simple: A case for using classical minimum norm estimation in the analysis of EEG and MEG data. *NeuroImage*, 21:1612–1621, 2004.
- [33] D. Higdon, J. Gattiker, B. Williams, and M. Rightley. Computer model calibration using high-dimensional output. *J. Amer. Statist. Assoc.*, 103:570–583, 2008.
- [34] R. A. Horn and C. R. Johnson. *Topics in Matrix Analysis*. Cambridge University Press, Cambridge, 1991.
- [35] H. Jeffreys. *Theory of Probability*. Oxford University Press, Cambridge, 3rd edition, 1961.
- [36] R. A. Johnson and D. W. Wichern. *Applied Multivariate Statistical Analysis*. Prentice Hall, Upper Saddle River, 6th edition, 2007.
- [37] J. Kaipio and E. Somersalo. *Statistical and Computational Inverse Problems*. Springer, New York, 2005.
- [38] Kutner, M. and Nachtsheim, C. and Neter, J. and Li, W. *Applied Linear Statistical Models*. McGraw-Hill/Irwin, Boston, 5th edition, 2005.
- [39] E. L. Lehmann and Casella, G. *Theory of Point Estimation*. Springer Science+Business Media, New York, 1998.
- [40] F. Lindgren, H. Rue, and J. Lindström. An explicit link between Gaussian fields and Gaussian Markov random fields: the stochastic partial differential equation approach. *J. R. Stat. Soc. Ser. B. Stat. Methodol.*, 73(4):423–498, 2011.
- [41] J. S. Liu. Metropolized independent sampling with comparisons to rejection sampling and importance sampling. *Statistics and Computing*, 6:113–119, 1996.
- [42] N. Metropolis, A. W. Rosenbluth, M. N. Rosenbluth, A. H. Teller, and E. Teller. Equation of state calculations by fast computing machines. *J. Chem. Phys.*, 21:1087–1091, 1953.
- [43] K. Mosegaard and A. Tarantola. Probabilistic Approach to Inverse Problems. In *International Handbook of Earthquake & Engineering Seismology, Part A.*, pages 237–265. Academic Press, 2002.
- [44] P. Müller. A generic approach to posterior integration and Gibbs sampling. Technical Report, Purdue University, 1991.
- [45] C. Nahkhleh, D. Higdon, C. K. Allen, and R. Ryne. Bayesian reconstruction of particle beam phase space. In *Bayesian Theory and Applications*, pages 673–686. Oxford University Press, 2013.
- [46] Omiros Papaspiliopoulos and Gareth O. Roberts. Non-Centered Parameterisations for Hierarchical Models and Data Augmentation. *Bayesian Statistics*, 7:307–326, 2003.
- [47] Omiros Papaspiliopoulos, Gareth O. Roberts, and Martin Sköld. A General Framework for the Parametrization of Hierarchical Models. *Statistical Science*, 22(1):59–73, 2007.
- [48] N. Petra, J. Martin, G. Stadler, and O. Ghattas. A computational framework for infinite-dimensional Bayesian inverse problems, part ii: stochastic Newton MCMC with application to ice sheet flow inverse problems. *SIAM J. Sci. Comput.*, 36(4):A1525–A1555, 2014.
- [49] N. G. Polson and J. G. Scott. Shrink globally, act locally: Sparse Bayesian regression and prediction. In J. M. Bernardo, M. J. Bayarri, J. O. Berger, A. P. Dawid, D. Heckerman, A. F. M. Smith, and M. West, editors, *Bayesian Statistics 9*, pages 501–538. Oxford University Press, 2010.
- [50] J. G. Propp and D. B. Wilson. Exact sampling with coupled Markov chains and applications to statistical mechanics. *Random Struct. Algor.*, 9:223–252, 1996.

- [51] C. E. Rasmussen and C. K. I. Williams. *Gaussian Processes for Machine Learning*. MIT Press, Cambridge, 2006.
- [52] S. I. Resnick. *A Probability Path*. Birkhäuser, Boston, 1999.
- [53] C. Robert and G. Casella. *Monte Carlo Statistical Methods*. Springer, New York, 2nd edition, 2004.
- [54] J. S. Rosenthal. Optimal proposal distributions and adaptive MCMC. In S. Brooks, A. Gelman, G. L. Jones, and X.-L. Meng, editors, *Handbook of Markov Chain Monte Carlo*, pages 93–111. Chapman & Hall/CRC, Boca Raton, 2011.
- [55] H. Rue and L. Held. *Gaussian Markov Random Fields*. Chapman & Hall/CRC, Boca Raton, 2005.
- [56] Y. Saad. *Numerical methods for large eigenvalue problems*, volume 158. SIAM, 1992.
- [57] A. K. Saibaba and P. K. Kitanidis. Efficient methods for large-scale linear inversion using a geostatistical approach. *Water Resour. Res.*, 48(5), 2012.
- [58] A. K. Saibaba and P. K. Kitanidis. Fast computation of uncertainty quantification measures in the geostatistical approach to solve inverse problems. *Adv. Water Resour.*, 82(0):124–138, 2015.
- [59] A. K. Saibaba, J. Lee, and P. K. Kitanidis. Randomized algorithms for generalized Hermitian eigenvalue problems with application to computing Karhunen–Loève expansion. *Numerical Linear Algebra with Applications*, 23(2):314–339, 2016.
- [60] T. J. Santner, B. J. Williams, and W. I. Notz. *The Design and Analysis of Computer Experiments*. Springer-Verlag, New York, 2003.
- [61] J. G. Scott and J. O. Berger. An exploration of aspects of Bayesian multiple testing. *J. Statist. Plann. Inference*, 136(7):2144–2162, 2006.
- [62] L. A. Shepp and B. F. Logan. The Fourier reconstruction of a head section. *IEEE Trans. Nucl. Sci.*, 21(3):21–43, 1974.
- [63] A. Spantini, A. Solonen, T. Cui, J. Martin, L. Tenorio, and Y. Marzouk. Optimal low-rank approximations of Bayesian linear inverse problems. *SIAM Journal on Scientific Computing*, 37(6):A2451–A2487, 2015.
- [64] A. M. Stuart. Inverse problems : A Bayesian perspective. *Acta Numer.*, 19(May):451–559, 2010.
- [65] G. C. Tiao and W. Tan. Bayesian analysis of random-effect models in the analysis of variance, I. Posterior distribution of variance components. *Biometrika*, 51:37–53, 1965.
- [66] J. A. Tropp, A. Yurtsever, M. Udell, and V. Cevher. Randomized single-view algorithms for low-rank matrix approximation. *arXiv preprint arXiv:1609.00048*, 2016.
- [67] van Dyk, D. and Park, T. Partially collapsed Gibbs samplers. *Journal of the American Statistical Association*, 103:790–796, 2008.

# Supplementary Material for Low Rank Independence Samplers in Bayesian Inverse Problems

D. Andrew Brown      Arvind Saibaba      Sarah Vallélian

This Supplementary Material contains additional material referenced in the manuscript that could aid the reader, but is not essential. We elaborate on possibilities for prior modeling of the precision (variance) components in the hierarchical model for the Bayesian inverse problem. We discuss also the use of noncentered parameterization in our proposed LRIS algorithm, supported by application to the 2D deblurring example. Supplementary Figures are at the end.

## 1 Priors on the Nuisance Parameters

Consider the Bayesian linear inverse problem with forward operator  $\mathbf{A} \in \mathbb{R}^{m \times n}$ , assuming independent observations with common precision  $\mu$ . We assume a Gaussian prior on the target  $\mathbf{x}$  to correspond to the  $L_2$  penalty in regularized inversion, with prior covariance matrix  $\mathbf{\Gamma}_{\text{pr}}$  known up to a multiplicative constant (precision)  $\sigma$ . Let  $\mathbf{b}$  denote the observed data. Then the model is

$$\begin{aligned} \mathbf{b} \mid \mathbf{x}, \mu &\sim \mathcal{N}(\mathbf{Ax}, \mu^{-1} \mathbf{I}) \\ \mathbf{x} \mid \sigma &\sim \mathcal{N}(\mathbf{0}, \sigma^{-1} \mathbf{\Gamma}_{\text{pr}}) \\ (\mu, \sigma) &\sim \Pi, \end{aligned} \tag{S1}$$

where  $\Pi$  is some distribution with support  $\mathbb{R}^+ \times \mathbb{R}^+$ . In the following, we consider two different specifications of  $\Pi$ .

### 1.1 Conditionally Conjugate Gamma Priors

The most straightforward case (and by far the most common) is to let  $\mu \sim \text{Gamma}(a_\mu, b_\mu)$  and  $\sigma \sim \text{Gamma}(a_\sigma, b_\sigma)$  independently, where we use the shape/rate parameterization of a Gamma distribution; e.g.,

$$\text{Gamma}(\mu \mid a, b) \propto \mu^{a-1} \exp(-b\mu), \quad \mu > 0.$$

With these Gamma prior models on  $\mu$  and  $\sigma$ , the joint posterior distribution of the model specified by (S1) is given by

$$\pi(\mathbf{x}, \mu, \sigma \mid \mathbf{b}) \propto \mu^{m/2+a_\mu-1} \sigma^{n/2+a_\sigma-1} \exp\left(-\frac{\mu}{2} \|\mathbf{Ax} - \mathbf{b}\|_2^2 - \frac{\sigma}{2} \|\mathbf{Lx}\|_2^2 - b_\mu \mu - b_\sigma \sigma\right). \tag{S2}$$

Since the elements of  $\mathbf{x}$  are expected to be highly correlated in the posterior, it is desirable to update  $\mathbf{x}$  all at once in a block Gibbs sampler. The full conditional distributions in this case are

$$\begin{aligned} \mathbf{x} \mid \mathbf{b}, \mu, \sigma &\sim \mathcal{N}(\mathbf{x}_{\text{cond}}, \mathbf{\Gamma}_{\text{cond}}) \\ \mu \mid \mathbf{b}, \mathbf{x}, \sigma &\sim \text{Gamma}\left(m/2 + a_\mu, \frac{1}{2} \|\mathbf{Ax} - \mathbf{b}\|_2^2 + b_\mu\right) \\ \sigma \mid \mathbf{b}, \mathbf{x}, \mu &\sim \text{Gamma}\left(n/2 + a_\sigma, \frac{1}{2} \|\mathbf{Lx}\|_2^2 + b_\sigma\right), \end{aligned} \tag{S3}$$

where  $\mathbf{\Gamma}_{\text{cond}} = (\mu \mathbf{A}^\top \mathbf{A} + \sigma \mathbf{\Gamma}_{\text{pr}}^{-1})^{-1}$  and  $\mathbf{x}_{\text{cond}} = \mu \mathbf{\Gamma}_{\text{cond}} \mathbf{A}^\top \mathbf{b}$ . The remaining question becomes specification of the hyperparameters in the Gamma priors.



To impose strong prior assumptions and to stabilize the MCMC algorithm, we can rescale the observed data with  $\tilde{\mathbf{b}} = \mathbf{b}/s_b$ , where  $s_b = \sqrt{(m-1)^{-1} \sum_{i=1}^m (b_i - \bar{b})^2}$  is the sample standard deviation. (See, for instance, [33].) In this case,  $\mathbb{V}(\tilde{\mathbf{b}})$  is expected to be reasonably close to one, though not exactly equal since correlation in the data induced by dependence on  $\mathbf{x}$  will cause  $s_b$  to over- or under-estimate the true standard deviation. After rescaling, an equivalent model to (S1) is

$$\tilde{\mathbf{b}} = \mathbf{A}\tilde{\mathbf{x}} + \tilde{\boldsymbol{\epsilon}}, \quad (\text{S4})$$

where  $\tilde{\mathbf{x}} = \mathbf{x}/s_b$  and  $\tilde{\boldsymbol{\epsilon}} \sim N(\mathbf{0}, \tilde{\mu}^{-1} \mathbf{I})$ . This is similar to the notion of a standardized regression model. (See, e.g., [38, Section 7.5].) In this case, we set the hyperparameters in the prior on  $\tilde{\mu}$  (or simply  $\mu$ , without loss of generality) to mildly concentrate the density about one; e.g.  $a_\mu = b_\mu = 1$ . By concentrating  $\mu$  about 1 and allowing  $\sigma$  to be vague with, say,  $a_\sigma = b_\sigma = 0.1$ , we are not restricting values of  $\lambda = \sigma/\mu$ , the corresponding regularization parameter in the MAP estimator with fixed  $\mu$  and  $\sigma$ . We remark, however, that in a fully Bayesian model the primary goal is to obtain an estimate of  $\mathbf{x}$ , so we are not really interested in  $\mu$  or  $\sigma$  in their own right (hence the name “nuisance parameters”).

Alternatively, notice that if  $\mu \sim \text{Gamma}(\epsilon, \epsilon)$ , then  $\pi(\mu) \propto \mu^{\epsilon-1} e^{-\epsilon\mu} \rightarrow \mu^{-1}$  as  $\epsilon \rightarrow 0$ . But  $\pi(\mu) = \mu^{-1}$  is the Jeffreys prior for a scale parameter and thus is invariant to reparameterization [10, Ch. 3]. For this reason it is common practice to set  $\epsilon$  to some small value in a  $\text{Gamma}(\epsilon, \epsilon)$  prior, say  $\epsilon = 0.1$  or  $\epsilon = 0.01$ , to approximate the behavior of the objective prior without sacrificing propriety or conjugacy. These are the priors we use in the 2D image deblurring example in Section 4.1 of the manuscript.

## 1.2 Weakly Informative Priors

Despite the convenience associated with the Gamma priors, it was observed by [23] that there is no limiting posterior distribution associated with taking  $\epsilon \rightarrow 0$  in a  $\text{Gamma}(\epsilon, \epsilon)$  prior, and that using such a hyperprior on the prior-level precision  $\sigma$  can sometimes yield undesirable behavior. (Although Carlin and Louis [15] remarked that it may not make a difference in terms of the estimand of interest,  $\mathbf{x}$ .) To rectify this, Gelman [23] proposed as a default prior the *folded- $t$*  distribution. This prior strikes a good compromise between a completely noninformative prior, which can lead to unreasonable estimates if the data are not informative about a parameter, and a strongly informative prior which prevents the data from ‘speaking for themselves’ in determining plausible *a posteriori* values. As such, it is called a “weakly informative” prior. Scott and Berger [61] proposed what has since become known as a “proper Jeffreys” prior [49] on the variance components. Defining  $\kappa^2 = \mu^{-1}$  and  $\tau^2 = \sigma^{-1}$ , the proper Jeffreys prior takes

$$\pi(\kappa^2, \tau^2) = (\kappa^2 + \tau^2)^{-2}, \quad \kappa^2, \tau^2 > 0.$$

This prior approximates the improper Jeffreys prior,  $\pi(\kappa^2, \tau^2) = (\kappa^2 + \tau^2)^{-1}$  [65]. Scott and Berger [61] remarked that the proper Jeffreys prior can be written as  $\pi(\kappa^2, \tau^2) = \kappa^{-2}(1 + \tau^2/\kappa^2)^{-2}\kappa^{-2} \equiv \pi(\tau^2 | \kappa^2)\pi(\kappa^2)$ , so that this model is equivalent to using the usual objective prior on the data-level variance while scaling the prior-level variance by  $\kappa^2$ , following the principle originally suggested by Jeffreys [35]. The conditional prior on  $\tau^2 | \kappa^2$  is also proper, an important consideration in finite mixture models, or when the data contain limited information about  $\tau^2$ . Lastly, it was observed by [12] that the proper Jeffreys prior is tail-equivalent to the prior obtained by placing a folded- $t_2$  on  $\tau$ , and thus is suitable as a default prior choice. For these reasons, this can be an attractive alternative to conjugate Gamma priors. In the CT example in Section 4.2 of the manuscript, we use the proper Jeffreys prior on the variance components. The sampling algorithm is not quite as simple since we no longer have conjugacy (see Appendix B of the manuscript), but we are still able to use our proposed low-rank independence sampler.

## 2 Non-Centered Parameterizations

In model (S1), the distribution of  $\mathbf{x}$  depends on  $\sigma$ , and the distribution of  $\mathbf{b}$  depends on  $\mathbf{x}$ , but  $\mathbf{b}$  is conditionally independent of  $\sigma$ , given  $\mathbf{x}$ . Under Gamma priors on  $\mu$  and  $\sigma$ , this yields convenient conditionally conjugate distributions for use inside a block Gibbs sampler, as discussed in Section 1.1 of the Supplementary Material. However, this also leads to high correlation between the  $\sigma$  and  $\mathbf{x}$  chains as the dimension of the problem increases, as noted by Bardsley [6] and Agapiou et al. [1].

A framework for potentially reducing the dependence between parameters in an MCMC algorithm is the so-called non-centered parameterization [46, 47]. A non-centered parameterization is one such that parameters are assigned *independent* prior distributions but still result in a model equivalent to the usual case, called a centered parameterization. The “centered” and “non-centered” terminology is a reference to the parameterizations considered by [21] for efficient sampling on normal linear mixed models, where certain parameters were centered or non-centered about other parameters.

Papaspiliopoulos et al. [47] argued that the best choice of parameterization depends on how well the underlying parameters are identified by the data. For our model, if the data were significantly informative about  $\mathbf{x}$  so that strong Bayesian learning occurred in the posterior, then a centered parameterization would likely be appropriate. On the other hand, if  $\mathbf{x}$  is only weakly identified by the data alone and hence more dependent on prior information, then there tends to be stronger correlation between  $\sigma$  and  $\mathbf{x}$  under the centered parameterization. In this case, a non-centered parameterization is likely the better option. Similar behavior was observed by Agapiou et al. [1], where it was shown that the performance of the non-centered parameterization breaks down as the data-level variance becomes small (i.e., the data become more reliable and thus contain more information about the solution). There exist also “partially non-centered” parameterizations, which can be estimated from the data when the appropriate parameterization to use is not clear [46, 47].

### 2.1 Implementation

To determine a non-centered parameterization for the hierarchical Bayesian inverse problem, we define a random variable  $\mathbf{z}$  independent of  $\sigma$  and express the distribution of  $\mathbf{x}$  in terms of these independent random variables. In our case, we have that  $\mathbf{x} \stackrel{d}{=} \sigma^{-1/2}\mathbf{z}$ , where  $\mathbf{z} \sim \mathcal{N}(\mathbf{0}, \mathbf{\Gamma}_{\text{pr}})$  independent of  $\sigma$ . Substituting this parameterization into (S1), the model becomes

$$\begin{aligned} \mathbf{b} \mid \mathbf{z}, \mu, \sigma &\sim \mathcal{N}(\sigma^{-1/2}\mathbf{A}\mathbf{z}, \mu^{-1}\mathbf{I}) \\ \mathbf{z} &\sim \mathcal{N}(\mathbf{0}, \mathbf{\Gamma}_{\text{pr}}) \\ \mu &\sim \text{Gamma}(a_\mu, b_\mu) \\ \sigma &\sim \text{Gamma}(a_\sigma, b_\sigma). \end{aligned} \tag{S5}$$

The joint posterior density is

$$\pi(\mathbf{z}, \mu, \sigma \mid \mathbf{b}) \propto f(\mathbf{b} \mid \mathbf{z}, \mu, \sigma) \pi(\mathbf{z}) \pi(\mu) \pi(\sigma), \tag{S6}$$

where  $f$  is the likelihood, and we adopt the conventional ambiguous use of  $\pi$ , understood to be defined by its arguments.

The conditional distributions for Gibbs sampling can be derived in a similar manner to the centered case discussed in Section 1.1 of the Supplementary Material, with the exception of  $\sigma$ . The non-centered parameterization loses the conditional conjugacy on this parameter, making an indirect sampling approach necessary. The conditional density of  $\mathbf{z}$  can be derived as the usual Normal-Normal model  $\mathbf{b} \sim \mathcal{N}(\mathbf{A}_\sigma \mathbf{z}, \mu^{-1}\mathbf{I})$  and  $\mathbf{z} \sim \mathcal{N}(\mathbf{0}, \mathbf{\Gamma}_{\text{pr}})$ , where  $\mathbf{A}_\sigma = \sigma^{-1/2}\mathbf{A}$ . Thus,

$$\mathbf{z} \mid \mathbf{b}, \mu, \sigma \sim \mathcal{N}(\mathbf{z}_{\text{cond}}, \mathbf{\Gamma}_{\text{cond}}),$$

where  $\mathbf{z}_{\text{cond}} = (\mu \mathbf{A}_\sigma^\top \mathbf{A}_\sigma + \mathbf{L}^\top \mathbf{L})^{-1} = ((\mu/\sigma) \mathbf{A}^\top \mathbf{A} + \mathbf{L}^\top \mathbf{L})^{-1}$  and  $\mathbf{z}_{\text{cond}} = \mu \mathbf{\Gamma}_{\text{cond}} \mathbf{A}_\sigma^\top \mathbf{b} = (\mu/\sigma^{1/2}) \mathbf{\Gamma}_{\text{cond}} \mathbf{A}^\top \mathbf{b}$ . One can easily show the same results for this parameterization as in the manuscript with appropriate

substitutions of  $\mu$  and  $\sigma$ . In particular, the same simplification of the MH acceptance ratio for the  $\mathbf{z}$  chain holds as in Proposition 1. The full conditional of  $\mu$  is also straightforward. It is derived similarly to the centered case:

$$\begin{aligned}\pi(\mu \mid \mathbf{b}, \mathbf{z}, \sigma) &\propto \mu^{m/2+a_\mu-1} \exp \left[ -\mu \left( \frac{1}{2} \|\mathbf{A}_\sigma \mathbf{z} - \mathbf{b}\|_2^2 + b_\mu \right) \right] \\ \Rightarrow \mu \mid \mathbf{b}, \mathbf{z}, \sigma &\sim \text{Gamma} \left( m/2 + a_\mu, \frac{1}{2} \|\mathbf{A}_\sigma \mathbf{z} - \mathbf{b}\|_2^2 + b_\mu \right).\end{aligned}$$

The most significant difference between the centered and non-centered parameterizations is the loss of conditional conjugacy on  $\sigma$ . The conditional density for  $\sigma$  is

$$\pi(\sigma \mid \mathbf{b}, \mathbf{z}, \mu) \propto \exp \left[ -\frac{\mu}{2} \|\sigma^{-1/2} \mathbf{A} \mathbf{z} - \mathbf{b}\|_2^2 \right] \sigma^{a_\sigma-1} e^{-b_\sigma \sigma}. \quad (\text{S7})$$

While there is no obvious simplification or standard distribution for  $\sigma$ , we can use a random walk Metropolis step to sample from it. Simplifying (S7) slightly, we have

$$\pi(\sigma \mid \mathbf{b}, \mathbf{z}, \mu) \propto \sigma^{a_\sigma-1} e^{-b_\sigma \sigma} \exp \left[ -\frac{\mu}{2\sigma} \left( \mathbf{z}^\top \mathbf{A}^\top \mathbf{A} \mathbf{z} - 2\sigma^{1/2} \mathbf{z}^\top \mathbf{A}^\top \mathbf{b} \right) \right], \quad \sigma > 0.$$

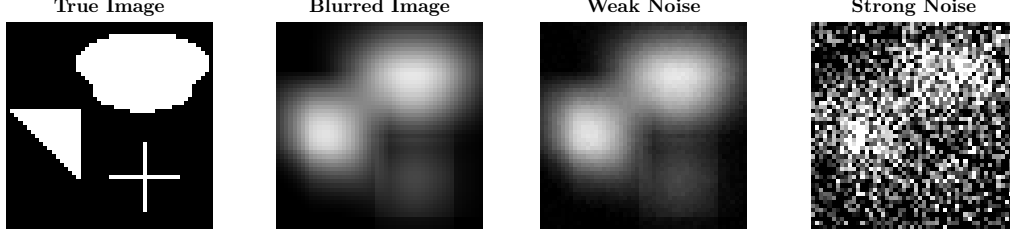
To eliminate boundary constraints on  $\sigma$  and thus facilitate Gaussian proposals in the Metropolis algorithm, reparameterize the model with  $\omega = \log(\sigma)$ . Then the density for  $\omega$  becomes

$$\pi_\omega(\omega \mid \mathbf{b}, \mathbf{z}, \mu) \propto e^{(a_\sigma-1)\omega - b_\sigma e^\omega} \exp \left[ -\frac{\mu}{2} \left( e^{-\omega} \mathbf{z}^\top \mathbf{A}^\top \mathbf{A} \mathbf{z} - 2e^{-\omega/2} \mathbf{z}^\top \mathbf{A}^\top \mathbf{b} \right) \right].$$

To implement the Metropolis step inside the block Gibbs algorithm, we can explicitly separate the burn-in phase from the sampling phase. During the first phase, we seek a suitable proposal distribution for  $\sigma$  (i.e., a suitable Gaussian proposal for  $\omega$ ). This is done by adaptively controlling the variance  $c$ , adjusting its scale based on the acceptance rate of the  $\sigma$  samples. A skeleton of this procedure is as follows:

1. Initialize  $c = c_0$  (say) and  $accept = 0$ .
2. For  $i \in (\text{burn-in iterations})$ 
  - (a) Draw  $\omega^* \sim N(\omega^{(i-1)}, c)$
  - (b) Accept/reject  $\omega^*$  according to the Metropolis ratio. If accepted,  $accept \leftarrow accept + 1$ .
  - (c) If  $i \bmod 100 = 0$ , then
    - i. If  $accept/100 < 0.35$ ,  $c \leftarrow 0.75c$ ,
    - ii. Else, if  $accept/100 > 0.5$ ,  $c \leftarrow 1.75c$
    - iii.  $accept \leftarrow 0$
  - (d) Repeat
3. For  $i \in (\text{sampling iterations})$ 
  - (a) Draw  $\omega^* \sim N(\omega^{(i-1)}, c)$ , where  $c$  is fixed at the value determined from the burn-in period.
  - (b) Accept/reject  $\omega^*$  according to the Metropolis ratio.
  - (c) Repeat

Agaipiou et al. [1] also considered a non-centered parameterization in a Bayesian Gaussian linear inverse problem, similar to that considered in this work. They relied on Metropolis sampling, but



Supplementary Figure 1: From left to right: target image, blurred image, reliable data, and corrupted data, used for comparing noncentered and centered parameterizations under low-rank independence sampling for 2D deblurring.

with a different proposal mechanism. Instead of sampling  $\sigma$  directly, they considered  $\zeta := \sigma^{-1/2}$ . After a change of variables, the full conditional distribution of  $\zeta$  is

$$\begin{aligned} \pi(\zeta \mid \mathbf{b}, \mathbf{z}, \mu) &\propto f(\mathbf{b} \mid \mathbf{z}, \mu, \zeta) \pi(\zeta) \\ &\propto \exp \left[ -\frac{\mu}{2} (\mathbf{b} - \zeta \mathbf{A} \mathbf{z})^\top (\mathbf{b} - \zeta \mathbf{A} \mathbf{z}) \right] \left( \frac{1}{\zeta^2} \right)^{a_\sigma + 1/2} e^{-b_\sigma / \zeta^2}. \end{aligned}$$

We see that the likelihood contribution to this density, written as a function of  $\zeta$ , is proportional to a Gaussian density. That is,

$$g(\zeta) := \exp \left[ -\frac{\mu}{2} (\mathbf{b} - \zeta \mathbf{A} \mathbf{z})^\top (\mathbf{b} - \zeta \mathbf{A} \mathbf{z}) \right] \propto \exp \left[ -\frac{\mu \mathbf{z}^\top \mathbf{A}^\top \mathbf{A} \mathbf{z}}{2} \left( \zeta - \frac{\mathbf{z}^\top \mathbf{A}^\top \mathbf{b}}{\mathbf{z}^\top \mathbf{A}^\top \mathbf{A} \mathbf{z}} \right)^2 \right], \quad (\text{S8})$$

which is the density of a normal distribution with mean  $\zeta_c := \mathbf{z}^\top \mathbf{A}^\top \mathbf{b} (\mathbf{z}^\top \mathbf{A}^\top \mathbf{A} \mathbf{z})^{-1}$  and variance  $\xi_c := (\mu \mathbf{z}^\top \mathbf{A}^\top \mathbf{A} \mathbf{z})^{-1}$ . Agaipiou et al. [1] use this Gaussian distribution as a proposal for an independence sampler, except that  $\zeta$  is restricted to be positive. In other words, their proposal distribution is a truncated Gaussian with density

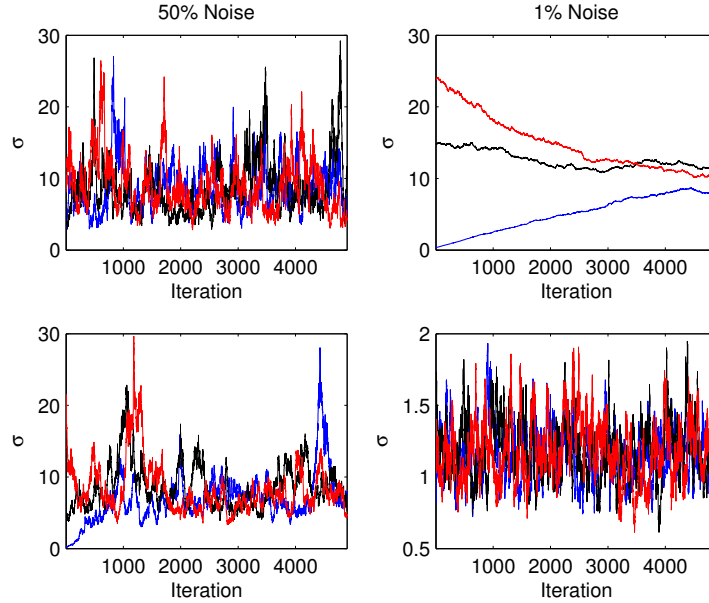
$$q(\zeta^*) = \mathcal{N}(\zeta^* \mid \zeta_c, \xi_c) \left( 1 - \Phi(-\zeta_c / \sqrt{\xi_c}) \right)^{-1},$$

where  $\Phi(\cdot)$  is the cumulative distribution function of the standard normal distribution. It is important to note that this approach assumes  $\mathbf{A}$  is of full rank, so that  $\mathbf{A} \mathbf{z} \neq \mathbf{0}$  for all  $\mathbf{z}$  (*a.e.*). In cases where  $\mathbf{A}$  is rank deficient, one can use the random walk Metropolis step previously discussed, but other approaches are possible.

## 2.2 Illustration with Image Deblurring

To illustrate use of the non-centered parameterization in LRIS, we consider again the 2D image deblurring example from Section 4.1 of the main manuscript. Here, the target image  $\mathbf{x}$  and the blurring operator  $\mathbf{A}$  are the same as before. However, we create two different observed datasets  $\mathbf{b}_i = \mathbf{A} \mathbf{x} + \epsilon_i$ ,  $i = 1, 2$ , with two different levels of noise. One set is strongly corrupted with 50% noise,  $\text{Var}(\epsilon_1) = 0.5^2 \|\mathbf{b}\|_\infty^2 \mathbf{I}$ , and the other contains much less noise,  $\text{Var}(\epsilon_2) = 0.01^2 \|\mathbf{b}\|_\infty^2 \mathbf{I}$ , and thus is more informative about the true solution  $\mathbf{x}$ . The target image, blurred image, and noisy data sets are displayed in Supplementary Figure 1.

For the centered parameterization, we use the same priors on  $\mathbf{x}, \mu$  and  $\sigma$  in model (S1) as in the manuscript, namely  $\Gamma_{\text{pr}}^{-1} = \mathbf{L}^\top \mathbf{L}$  with  $\mathbf{L} = -\Delta + \delta \mathbf{I}$  and  $\epsilon = 0.1$  in the  $\text{Gamma}(\epsilon, \epsilon)$  priors on  $\mu$  and  $\sigma$  to approximate scale invariant objective priors, and use the same low-rank Metropolis-Hastings-within-Gibbs algorithm as in the manuscript. To implement the non-centered parameterization, we use our proposed low-rank independent sampler to update  $\mathbf{x}$  and the independent sampler proposed by [1] to update  $\sigma^{-1/2}$ . Our interest here is not in posterior inference about the target image, but



Supplementary Figure 2: Trace plots of the  $\sigma$  chains obtained from centered and non-centered parameterizations using both datasets displayed in Supplementary Figure 1. The left column corresponds to the noisy data and right column to the reliable data. The top row are plots obtained from the noncentered parameterization, and the bottom row is obtained from the centered parameterization.

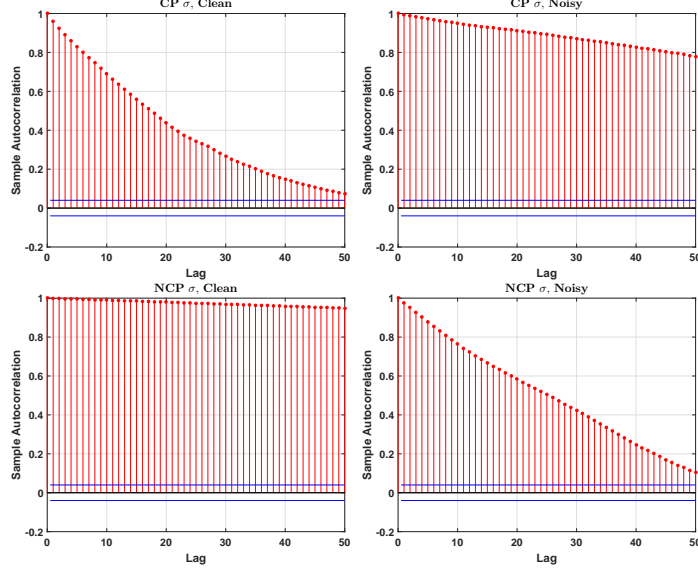
in the mixing behavior of these two parameterizations applied to data with different amounts of noise. Thus, rather than running to and diagnosing convergence, we run only 5,000 iterations of each Markov chain to study autocorrelation and how quickly the chains appear to be moving through their support. Under each configuration, we run three chains in parallel, with  $\mu$  and  $\mathbf{x}$  initialized by drawing them randomly from their prior distributions. The prior precision  $\sigma$  is initialized at 0.1, 6, and 25 for chains 1, 2, and 3, respectively.

Supplementary Figure 2 displays the trace plots of the three  $\sigma$  chains under each of the four combinations of data and parameterization. With severely noisy data, we see that the noncentered parameterization shows stronger mixing than the centered parameterization, and the opposite is true with the reliable data containing only 1% noise. The differences under the reliable data are particularly striking, where we see improvement in the centered parameterization but a very severe degradation in performance of the noncentered parameterization. The drift in all of the chains is indicative of considerable autocorrelation, and this is confirmed by examining the autocorrelation functions plotted in Supplementary Figure 3 and the estimated lag 1 and lag 50 correlation coefficients in Supplementary Table 1. Each chain suffers from high lag 1 autocorrelation, but it decays quicker under the non-centered parameterization for the noisy data, and quicker for the centered parameterization under the more reliable data. The decay of the autocorrelation is particularly poor for the noncentered parameterization with the reliable data.

	<u>Reliable</u>		<u>Noisy</u>	
	Lag 1	Lag 50	Lag 1	Lag 50
CP	0.968	0.174	0.995	0.774
NCP	0.999	0.974	0.982	0.348

Table 1: Estimated autocorrelation coefficients of one  $\sigma$  chain, for each data / parameterization combination in Supplementary simulation study.

The results of this illustration demonstrate the ease with which either the non-centered or cen-



Supplementary Figure 3: Estimated autocorrelation functions of one  $\sigma$  chain from the Supplementary simulation study, each obtained from centered (top row) and non-centered (bottom row) parameterizations using both weakly (left column) and strongly (right column) corrupted data.

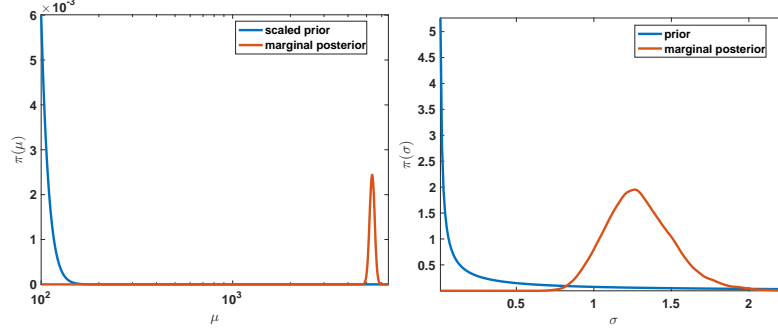
tered parameterization can be used in combination with our proposed low-rank independence sampler. Further, the relative performance of non-centered versus centered parameterizations previously observed in [46, 47, 1] is still present when using our more computationally efficient alternative. In particular, for strongly corrupted data,  $\mathbf{x}$  is more strongly determined through the prior than the data, so that a non-centered parameterization is preferable. More reliable data impose the approximate constraint that  $\mathbf{b} \approx \sigma^{-1/2} \mathbf{A}\mathbf{z}$ , severely degrading the performance of the non-centered parameterization. Thus, when using our proposed approach, a practitioner can still appeal to the same considerations when choosing a more effective parameterization for convergence of their MCMC algorithm.

### 3 Supplementary Figures

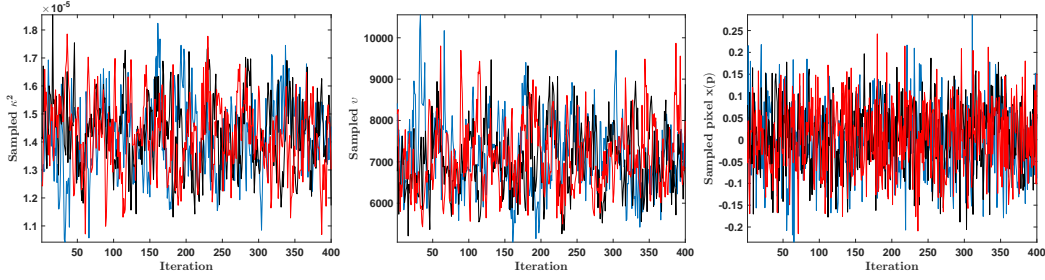
In Supplementary Figure 4, we compare the (vague) Gamma priors on  $\mu$  and  $\sigma$  with the marginal posterior distributions estimated from the MCMC samples of the joint posterior. The prior for  $\mu$  has been scaled by a factor of 10,000 for visualization. Note the significant difference between the distributions, indicating that strong Bayesian learning has occurred.

Here we present the convergence diagnostics for the CT example of Section 4.2. Trace plots of the samples from the thinned MCMC chains using weakly informative priors are displayed in Supplementary Figure 5, and autocorrelation plots are displayed in Supplementary Figure 6. In Supplementary Figure 7, we plot the cumulative averages of the parameters  $\kappa^2$  and  $\nu$  of these samples. The PSRFs for these parameters were both 1.00. Even after thinning, we see some correlation between the samples.

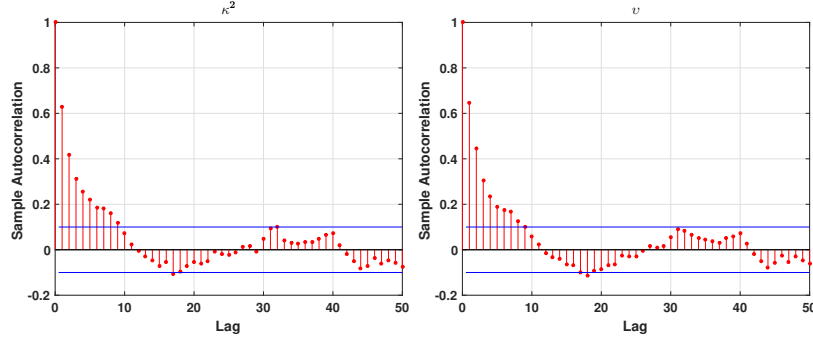
We next present convergence diagnostics for the CT example with conjugate Gamma prior models instead of proper Jeffreys, to justify the comparison in the manuscript. We use vague Gamma priors for  $\mu$  and  $\sigma$  as in the 2D example, and the same prior for  $\mathbf{x}$  as in the original CT experiment. We again use the largest 4900 eigenvalues, computed using the randomized SVD, in the low-rank proposal distribution for  $\mathbf{x}$ . We simulate three (randomly initialized) Markov chains using the MCMC



Supplementary Figure 4: Priors and marginal posterior distributions for  $\mu$  (left) and  $\sigma$  (right) in the 2D deblurring example.

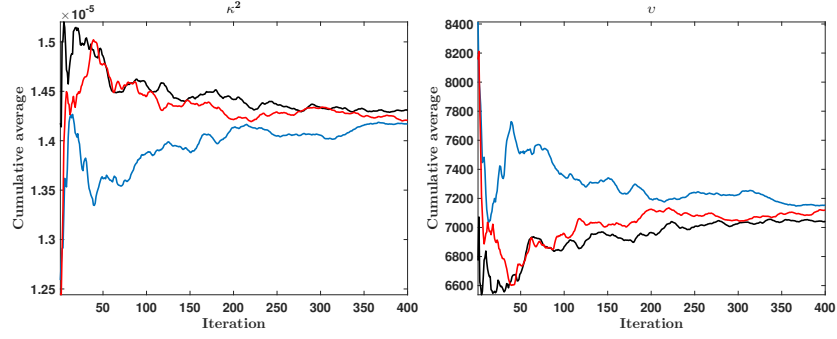


Supplementary Figure 5: Trace plots for the thinned chains in the CT image reconstruction example. Left: noise variance  $\kappa^2$ . Center: Variance ratio  $v = \tau^2/\kappa^2$ . Right: A randomly chosen pixel of the image  $\mathbf{x}$ .

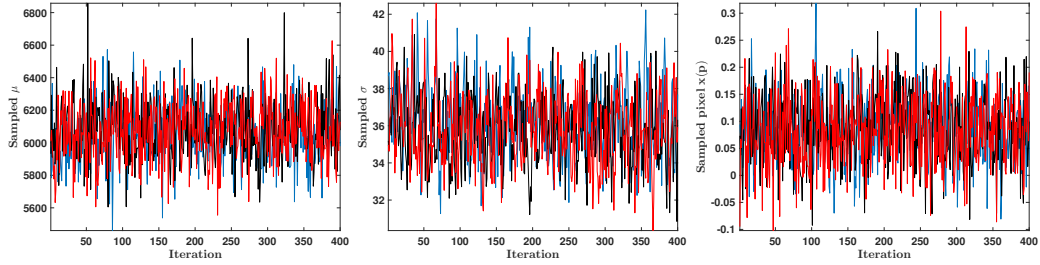


Supplementary Figure 6: Autocorrelation plots for the thinned chains in the CT image reconstruction example. Left: noise variance  $\kappa^2$ . Right: Variance ratio  $v = \tau^2/\kappa^2$ .

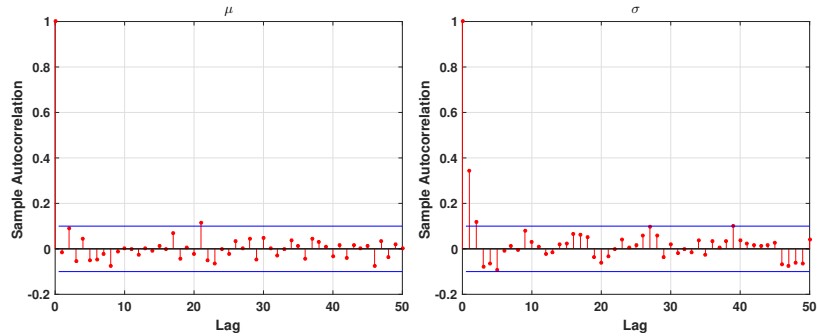
algorithm with our proposed approach for 20,000 iterations. These chains are then thinned and the burn-in period discarded to generate an equal sample size as in the previous experiment. Trace plots, autocorrelation plots, and PSRFs were used to determine approximate convergence of the chains. The trace plots are displayed in Supplementary Figure 8 and the autocorrelation plots for  $\mu$  and  $\sigma$  are in Supplementary Figure 9. The PSRFs for  $\mu$  and  $\sigma$  were 1.00 and 1.01 respectively.



Supplementary Figure 7: Cumulative averages of  $\kappa^2$  and  $v$  for each of the thinned MCMC chains in the CT example.



Supplementary Figure 8: Trace plots for the three thinned chains using Gamma priors in the CT image reconstruction example. Left: noise precision  $\mu$ . Center: prior precision  $\sigma$ . Right: a randomly chosen pixel of the image  $\mathbf{x}$ .



Supplementary Figure 9: Autocorrelation plots for one thinned chain using Gamma priors in the CT image reconstruction example. Left: noise precision  $\mu$ . Right: prior precision  $\sigma$ .